GCA TECHNICAL REPORT NO. 64-10-N

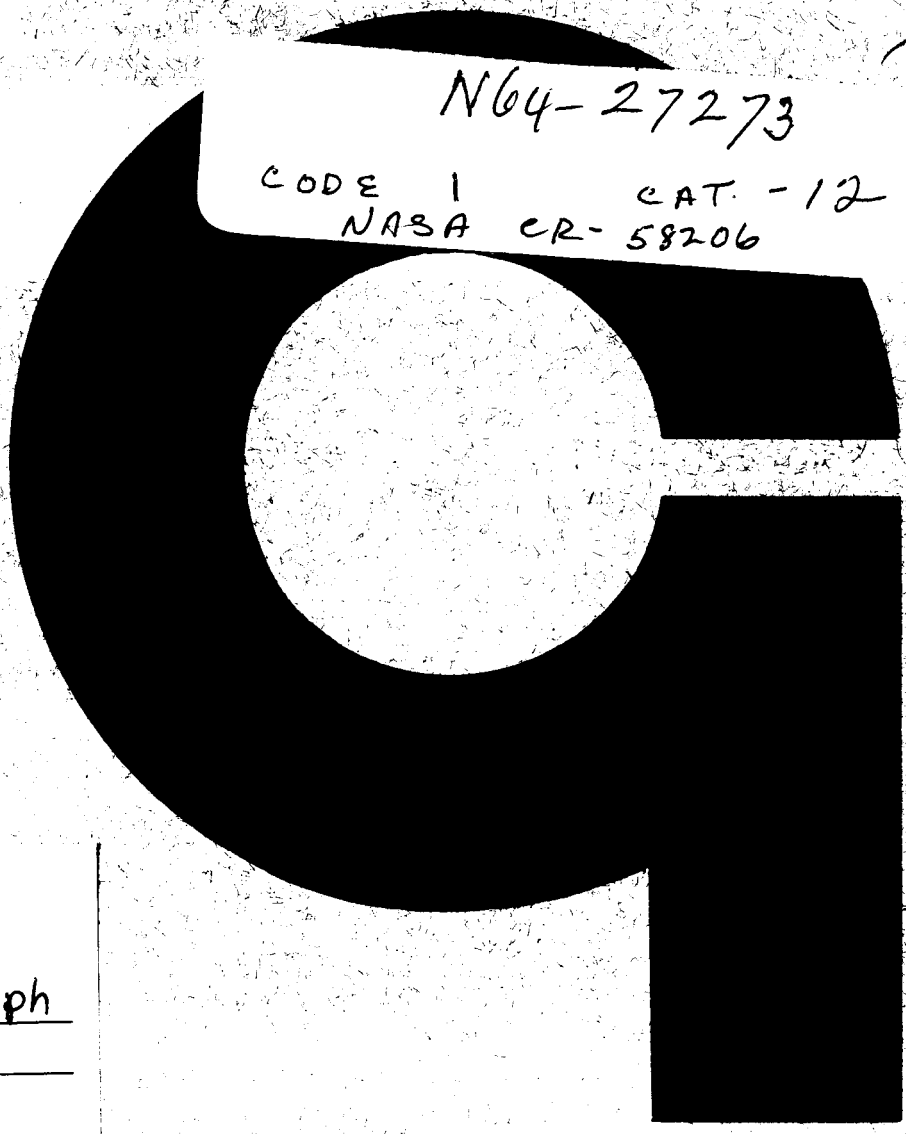

EXPERIMENTAL STUDY ON THE DYNAMICS AND STRUCTURE OF THE UPPER ATMOSPHERE

FINAL REPORT

CONTRACT NO. NASw-712

PREPARED FOR

NATIONAL AERONAUTICS AND SPACE ADMINISTRATION

WASHINGTON 25, D.C.

JUNE 1964

GEOPHYSICS CORPORATION OF AMERICA BEDFORD, MASSACHUSETTS

GCA Technical Report No. 64-10-N

EXPERIMENTAL STUDY ON THE DYNAMICS AND STRUCTURE OF THE UPPER ATMOSPHERE

Contract No. NASw-712

FINAL REPORT

June 1964

GEOPHYSICS CORPORATION OF AMERICA
Bedford, Massachusetts

Prepared for

NATIONAL AERONAUTICS AND SPACE ADMINISTRATION
Washington 25, D. C.

TABLE OF CONTENTS

SECTION 1

INTRODUCTION

The purpose of this contract was to measure upper atmospheric winds and diffusivity from analysis of the motions of trails of sodium and lithium vapor which are ejected from sounding rockets during twilight. A major specific objective of the contract was participation in an international program for worldwide measurement of winds. A total of nine vapor trail payloads were prepared for three different launch sites. Other specific objectives of the contract were the investigation of atmospheric turbulence through analysis of the vapor trails around 100 km altitude where the growth rate is often rapid and irregular, and the investigation of methods to determine atmospheric temperatures from the vapor trails.

Complete descriptions of the experimental and analytical methods employed are given in reports covering NASA contract NAS5-215 and NASw-396.[1,2,3,4] Primary data is taken photographically from several widely separated locations. Triangulation methods are used to determine winds which are defined as the direction and rate of the vapor trail movement. Densitometer measurements of the trail width are used to determine

expansion characteristics and diffusion coefficients. The accumulation of data and continuing analysis has resulted in new hypotheses concerning the wind structure and related phenomena. A new model of the structure of winds between 85 and 135 km was constructed from the experimentally determined values obtained at Wallops Island, Virginia and Sardinia, Italy. The model is consistent with data collected by the radio-meteor method, but presents an entirely new picture in which the total amplitude of the wind at a given height can be attributed to periodic, tidal or thermal driving forces. The irregular structure and rapid growth of the vapor trails around 100 km altitude is not explained by existing turbulence theories. Results of detailed analysis of trail growth in this region suggest that new or different explanations may be required. Detailed analysis of the relation of wind structure and "Sporadic E" also indicate serious deficiencies in existing theories.

SECTION 2

ROCKET FIRINGS

A total of nine vapor payloads were constructed on this contract and three were fired at each of the following launch sites: (1) Wallops Island, Virginia (37°50' N, 75°29' W), (2) Fort Churchill, Canada (58° 44' N, 93°49' W), (3) Eglin A.F.B., Florida (29°36' N, 86°36' W). The launchings at Eglin A.F.B. were conducted under the direction of R. Rosenberg of AFCRL. The payloads and one representative to assist in the prelaunch preparation were supplied under this contract. The results of these firings are being reported by that agency.[5,6,7] Collections and analysis of data from the Wallops Island and Fort Churchill firings were performed under this contract and results are reported here. Firings from all sites were to occur during a specified period as part of an international program for measurement of winds. Actual firing times and results are summarized in Table 1. The failure to eject vapor during the morning of 24 May has not been explained.

Another series of firings occurred during January 1964. This series was sponsored under contract NAS5-3434, but studies of turbulence and diffusion were conducted under contract NASw-712. The series consisted

TABLE 1

ROCKET FIRINGS

Launch Site	NASA No.	Date	Time (Zulu)	Peak Altitude (km)
Ft. Churchill	14.13 CA	22 May 63	0410	200
Ft. Churchill	14.14 CA	22 May 63	0751	185
Ft. Churchill	14.15 CA	23 May 63	0413	185
Wallops Island	14.40 CA	24 May 63	0045	205
Wallops Island	14.41 CA	24 May 63	0900	---
Wallops Island	14.42 CA	25 May 63	0047	197
Wallops Island	14.38 CA	15 January 64	2234	50
Wallops Island	14.106 CA	15 January 64	2240	114
Wallops Island	14.125 CA	16 January 64	0500	170
Wallops Island	14.126 CA	16 January 64	1134	198

of four firings at Wallops Island. Results from two of these during evening twilight on 15 January were seriously effected by rocket malfunction and did not reach sufficient altitudes for useful diffusion or turbulence data. One of the rockets was fired at local midnight and though a chemiluminescent trail was produced and winds were determined, no diffusion or turbulence data was obtained. The fourth rocket was fired during morning twilight and useful observations for diffusion and turbulence studies were recorded. This data will be discussed in another section of this report. A summary of these firings is also given in Table 1.

SECTION 3

WIND DATA

The standard 70 mm cameras were used for the Wallops firings. Camera sites at Dover Air Force Base, Camp A.P. Hill, Andrews Air Force Base, and Dam Neck Naval Station were used. Wind data were reduced with the analog reduction system.[1]

Modified K-24 cameras were used at Fort Churchill. Sites were established at Eskimo Point, Seal River, Belcher, Twin Lakes, and the launch area. These site locations are shown in Figure 1.

Winds were determined by noting the motion of discernible features of the clouds. The positions of these features for a specific time were computed from photographic plate coordinates using triangulation techniques.

The wind profiles for the five firings are given in Figures 2-11. For each flight, wind speed and direction of transport of the sodium trail are given as a function of altitude on separate plots. Dates on the figures are based on standard time.

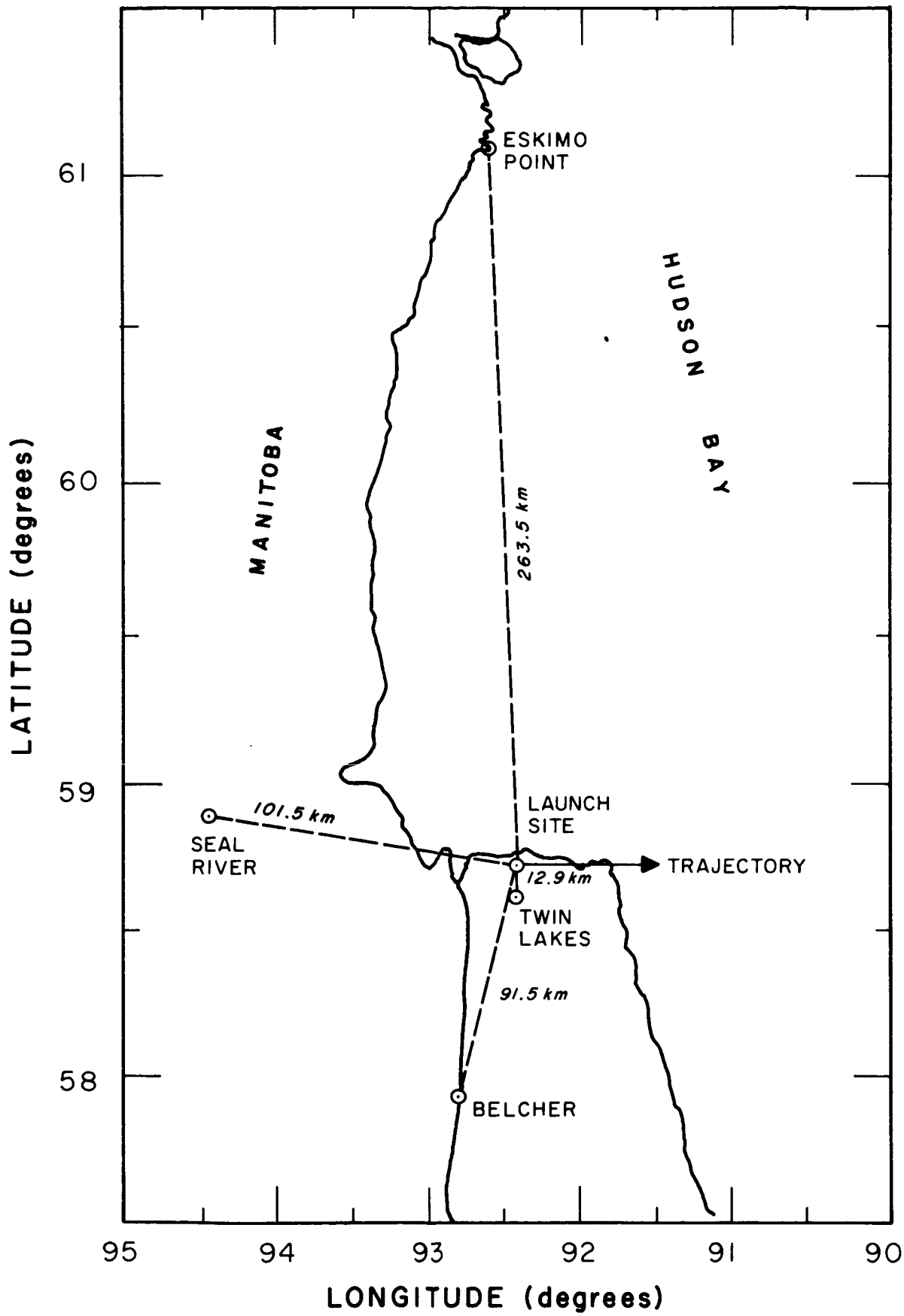

Figure 1. The geographic location of the launch site and the four observing sites, Eskimo Point, Seal River, Belcher, and Twin Lakes.

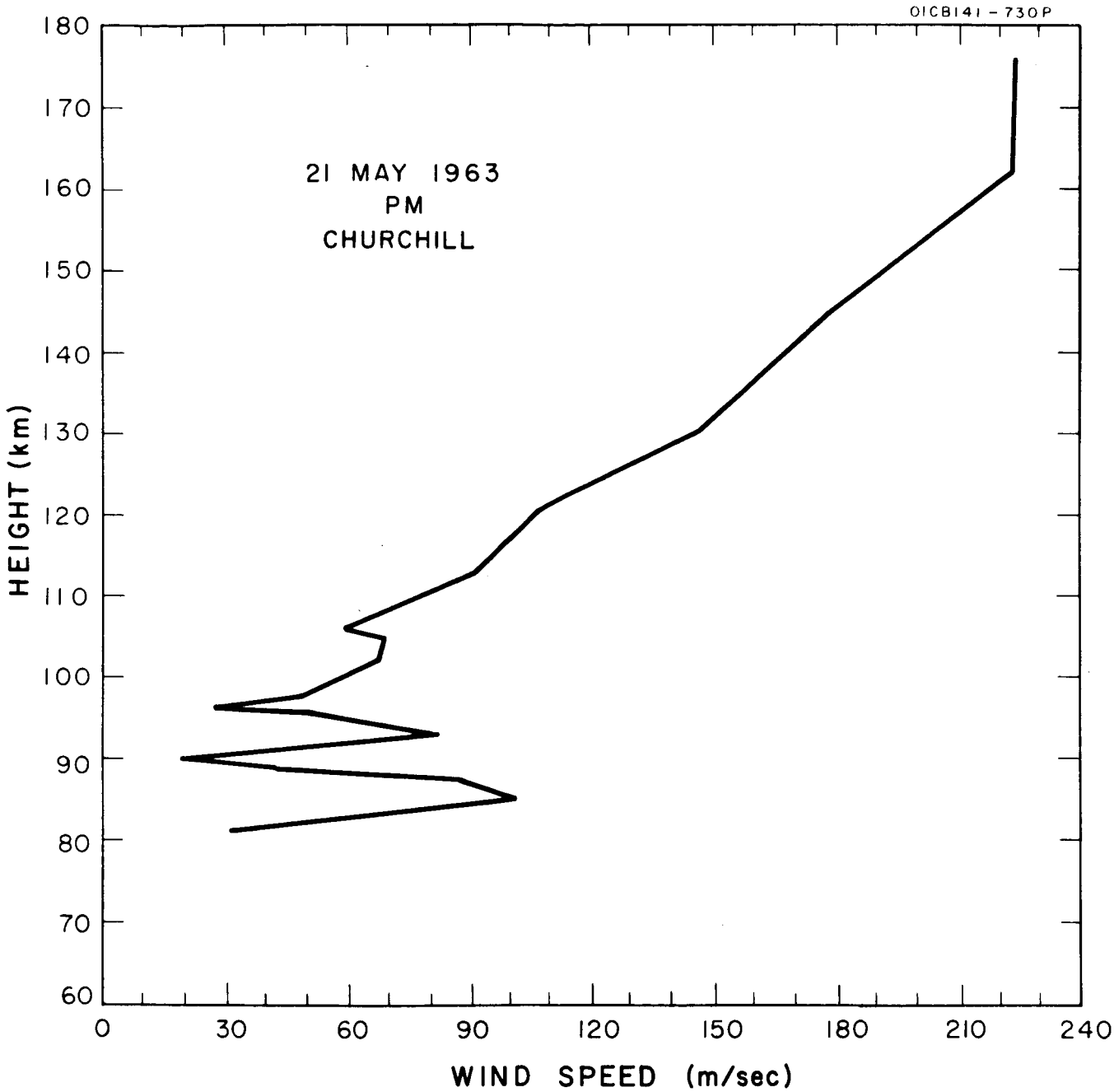

Figure 2. Wind speed as a function of height for evening twilight of 21 May 1963 at Churchill.

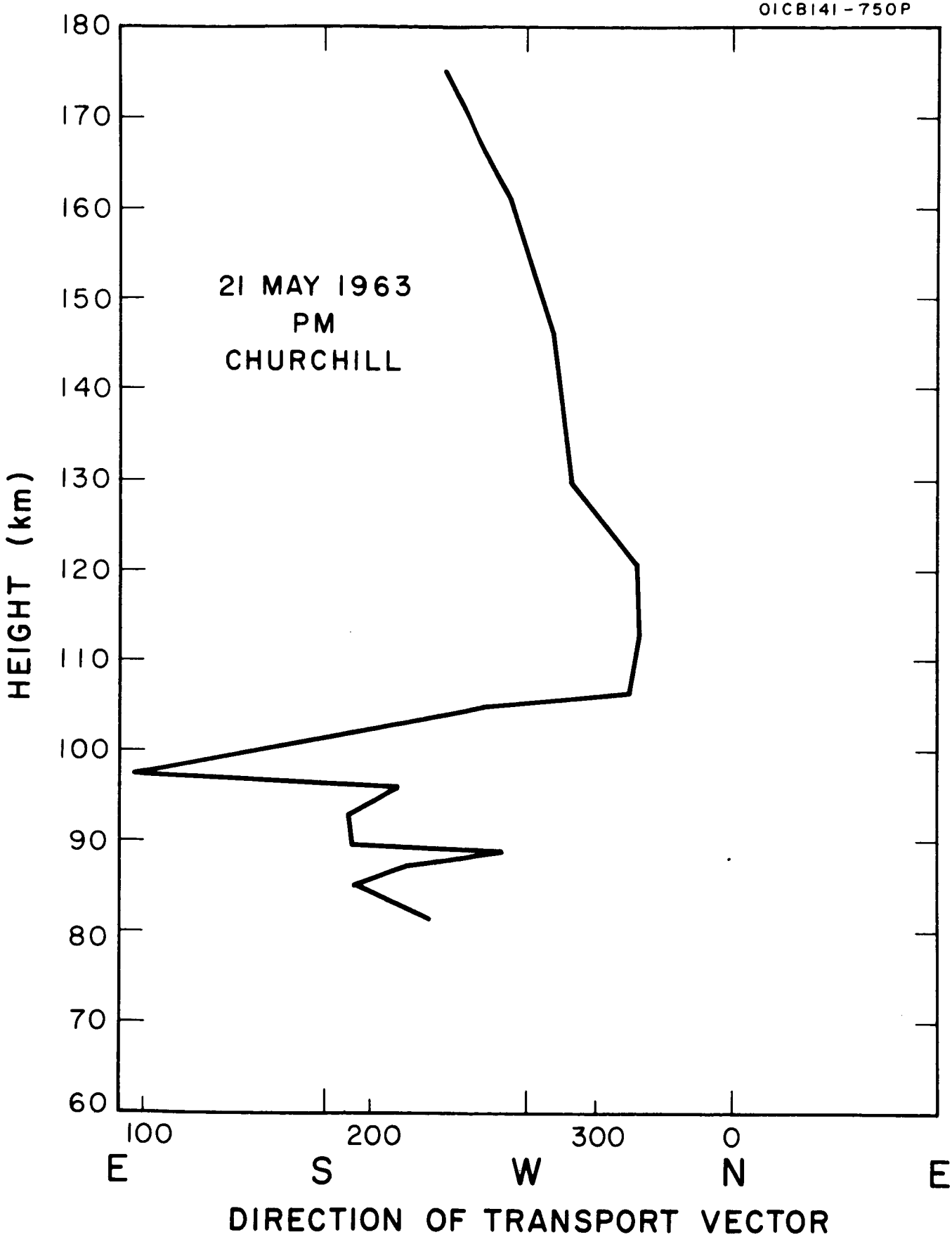

Figure 3. Direction of transport vector as a function of height for evening twilight of 21 May 1963 at Churchill.

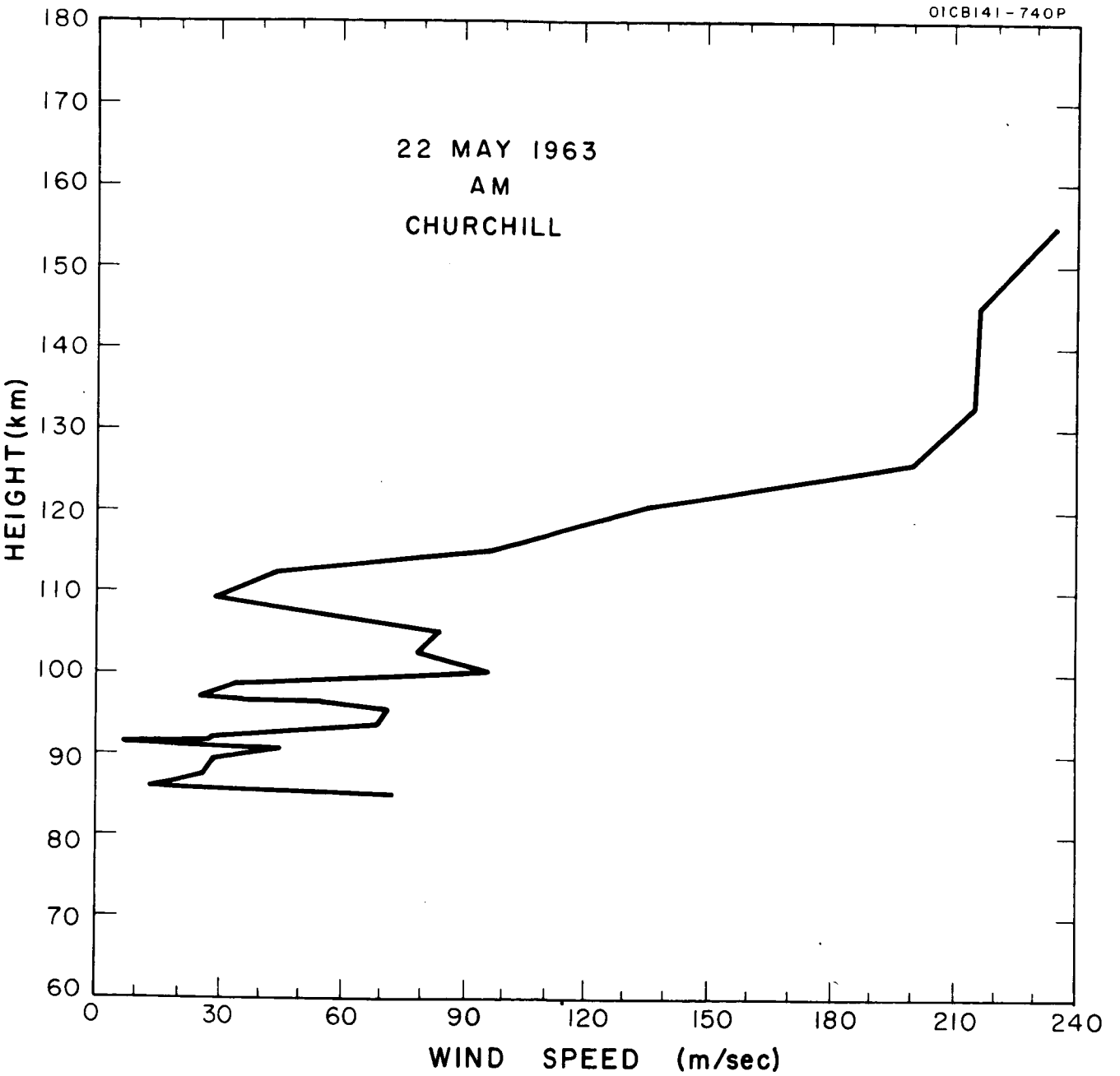

Figure 4. Wind speed as a function of height for morning twilight of 22 May 1963 at Churchill.

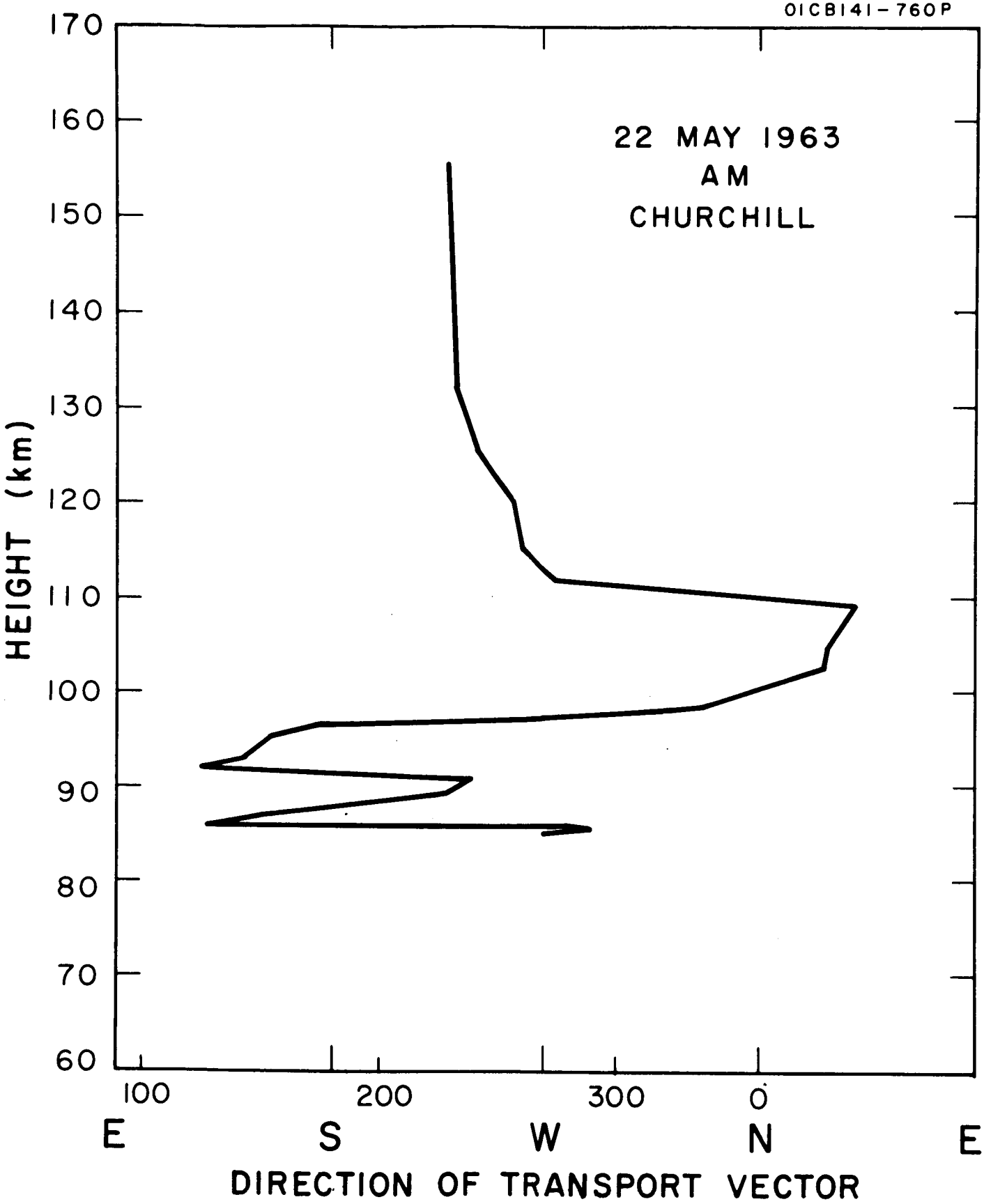

Figure 5. Direction of transport vector as a function of height for morning twilight of 22 May 1963 at Churchill.

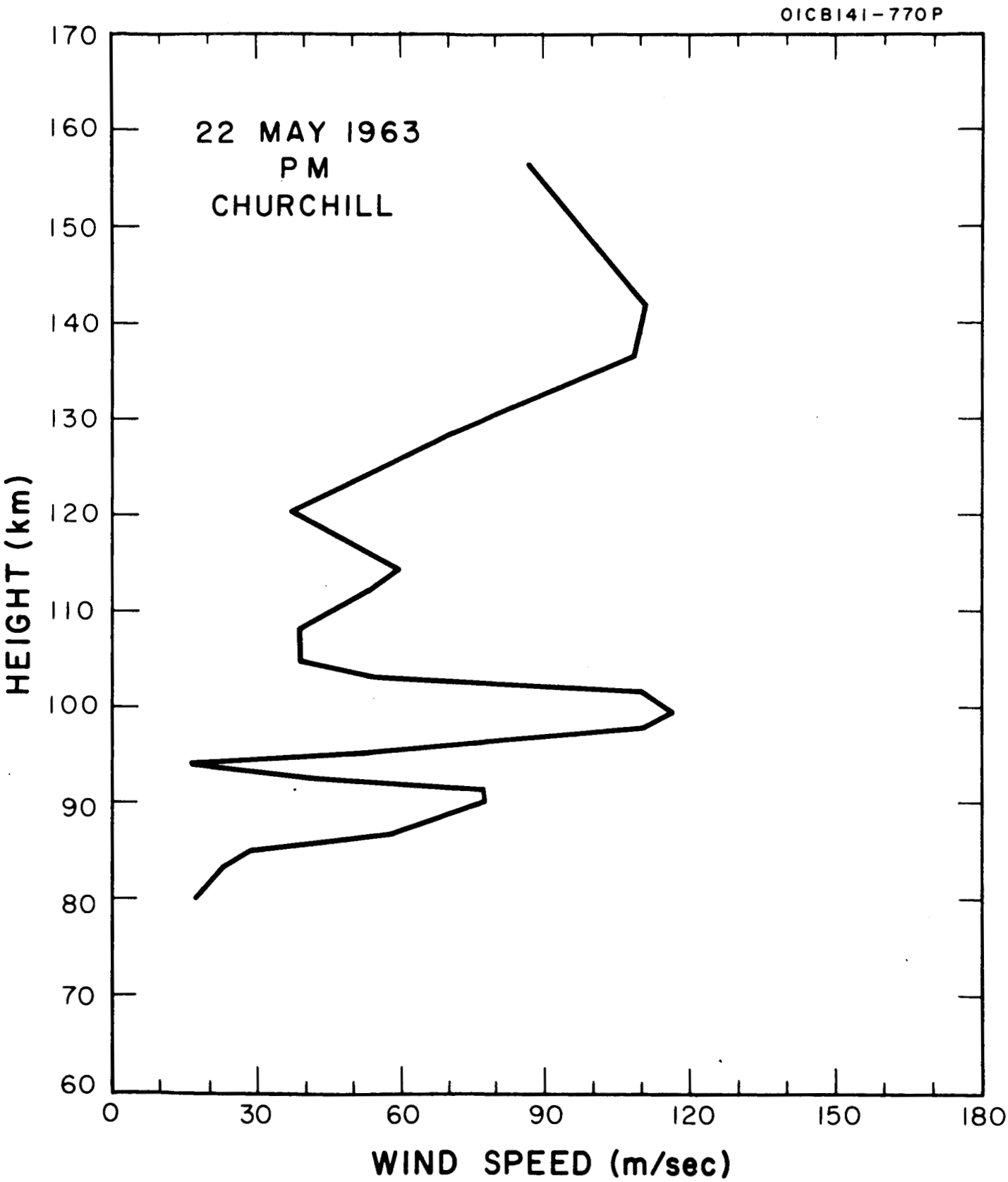

Figure 6. Wind speed as a function of height for evening twilight of 22 May 1963 at Churchill.

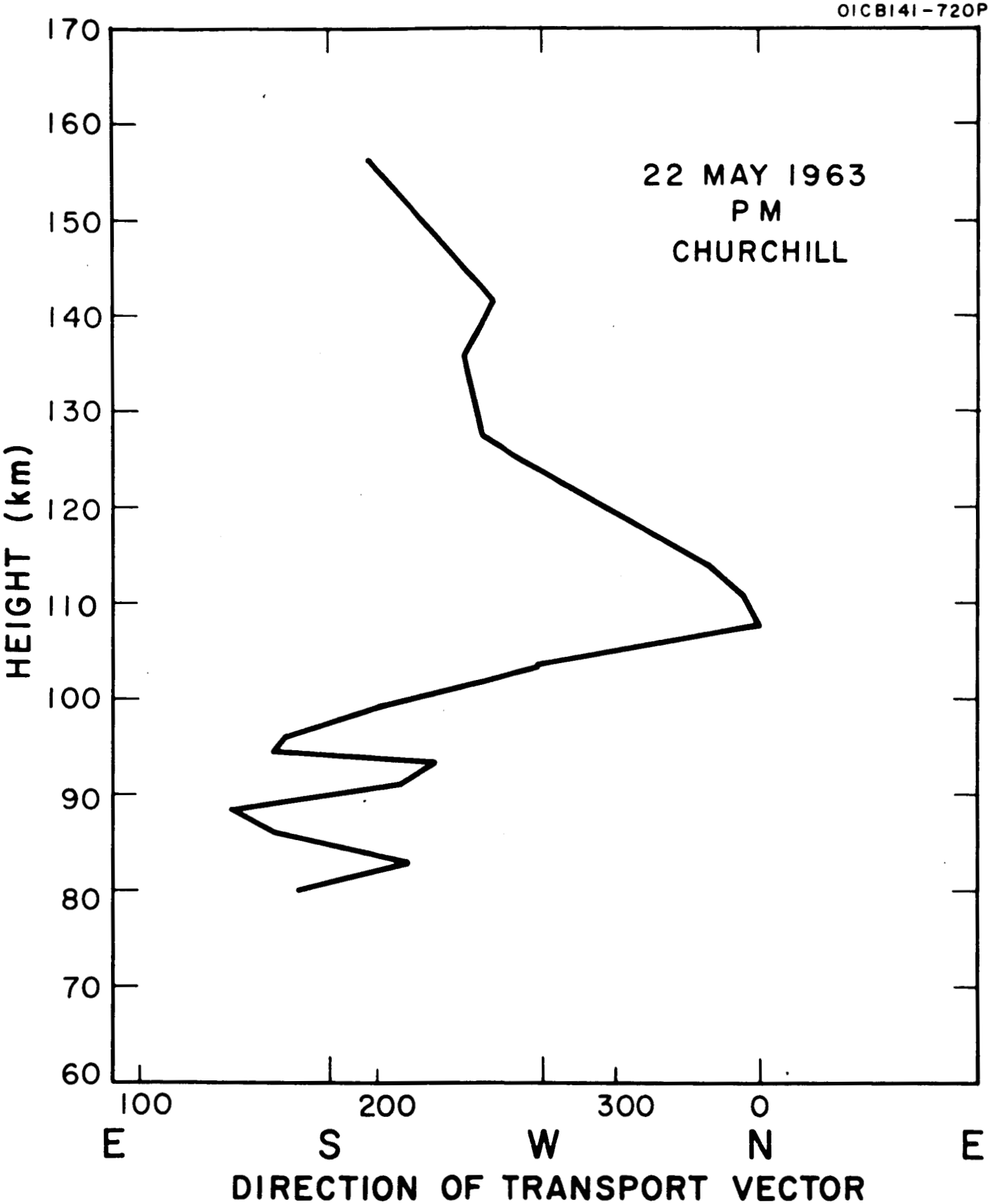

Figure 7. Direction of transport vector as a function of height for evening twilight 22 May 1963 at Churchill.

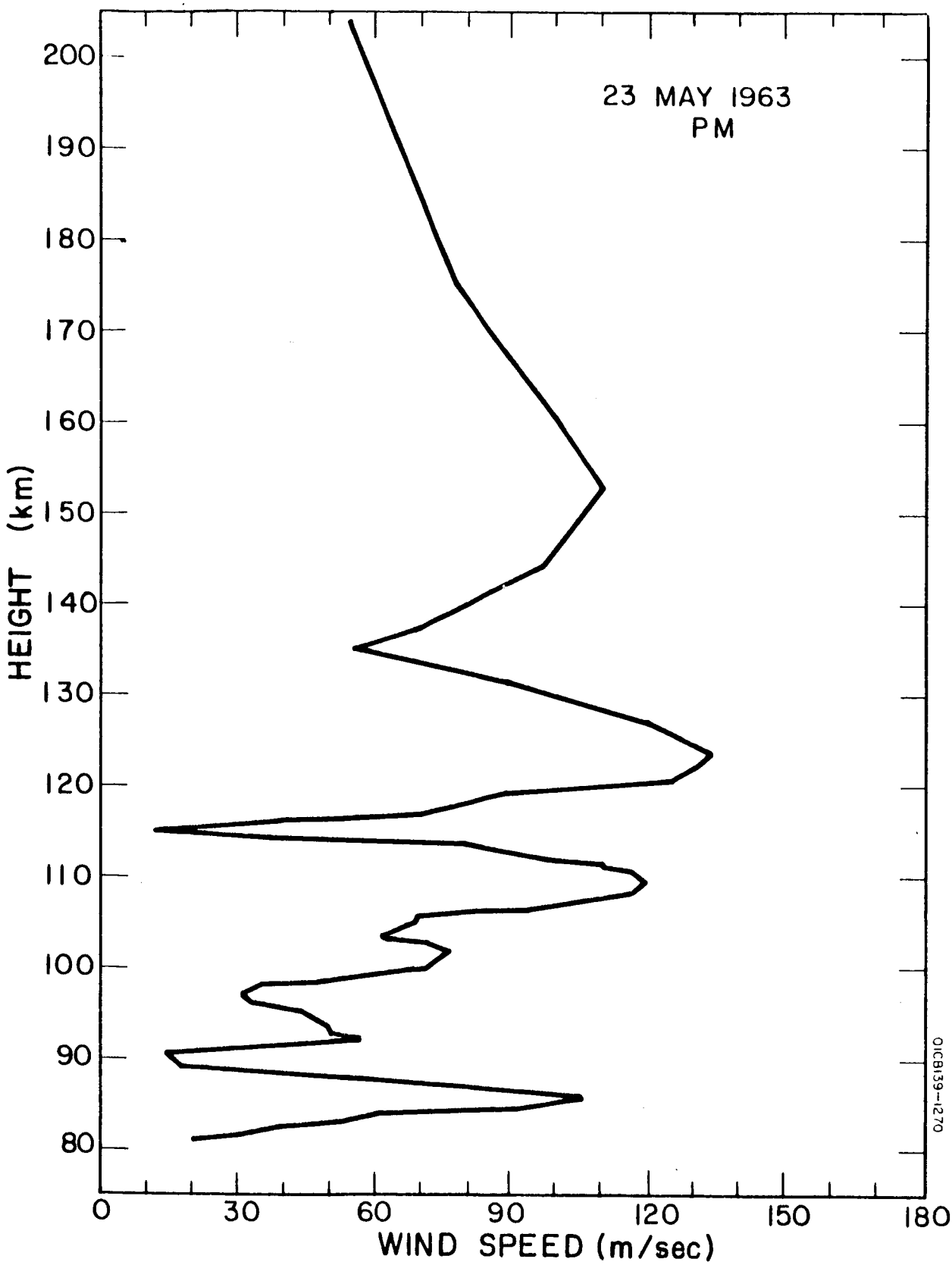

Figure 8. Wind speed as a function of height for evening twilight of 23 May 1963 at Wallops.

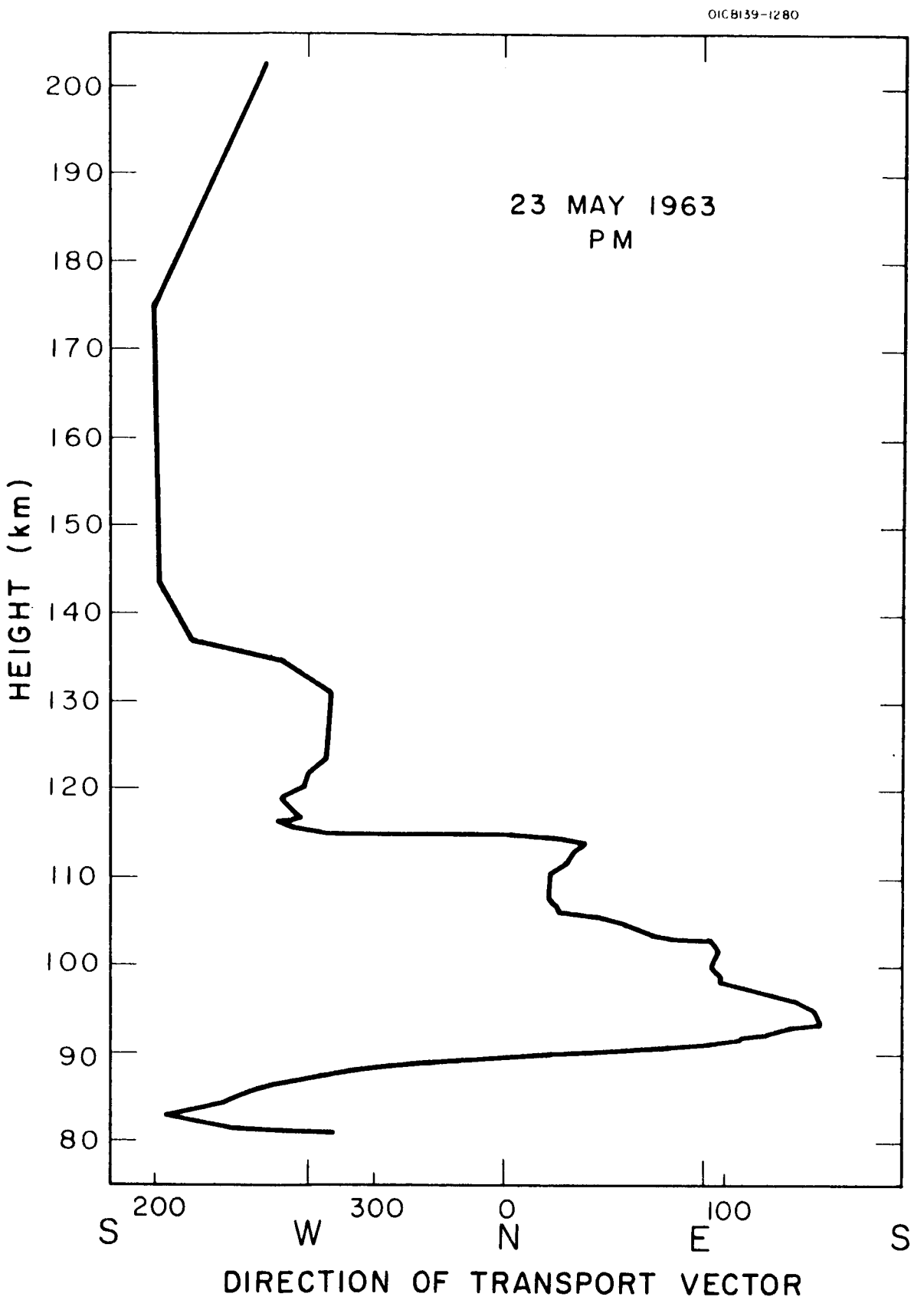

Figure 9. Direction of transport vector as a function of height for evening twilight of 23 May 1963 at Wallops.

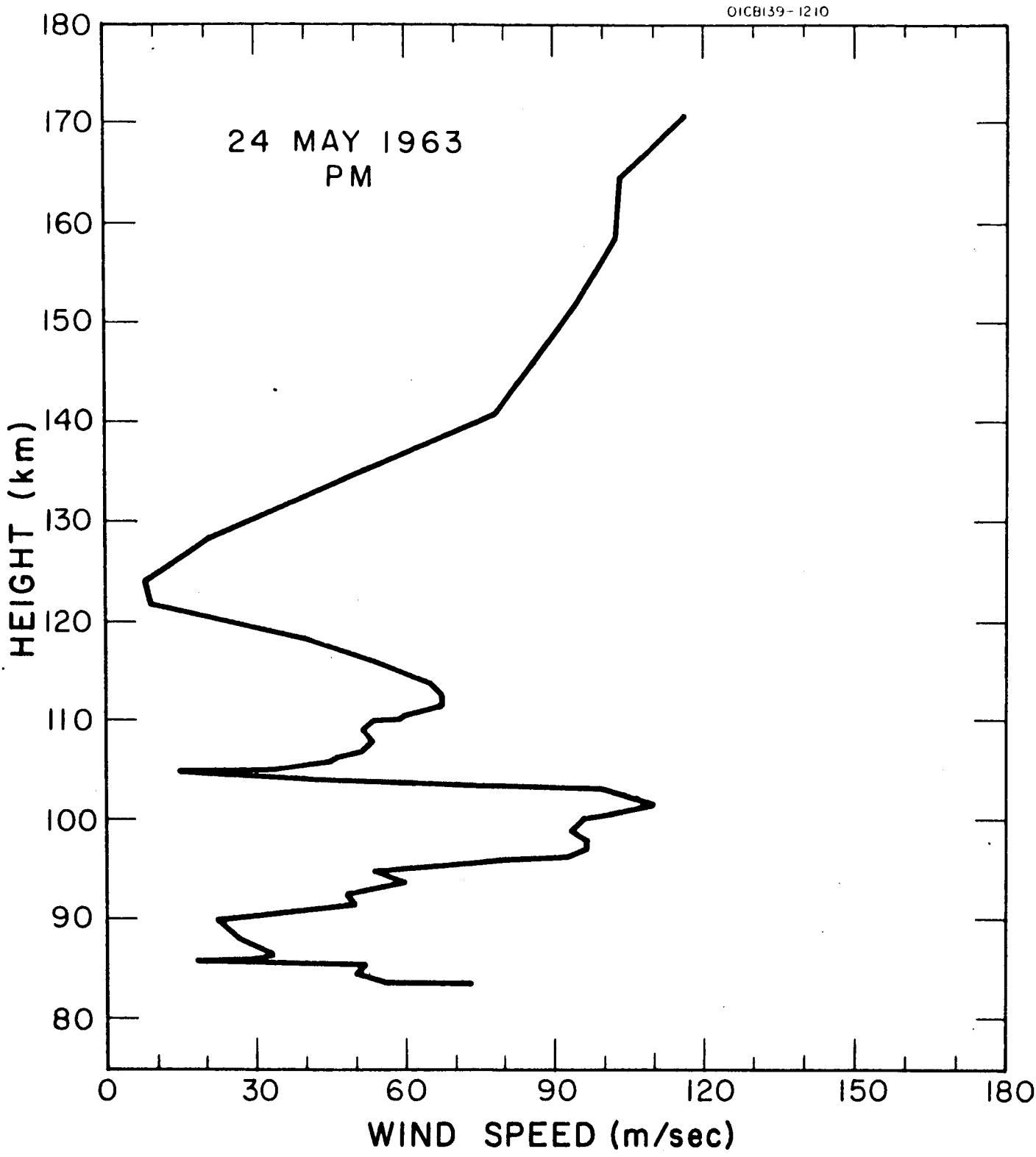

Figure 10. Wind speed as a function of height for evening twilight of 24 May 1963 at Wallops.

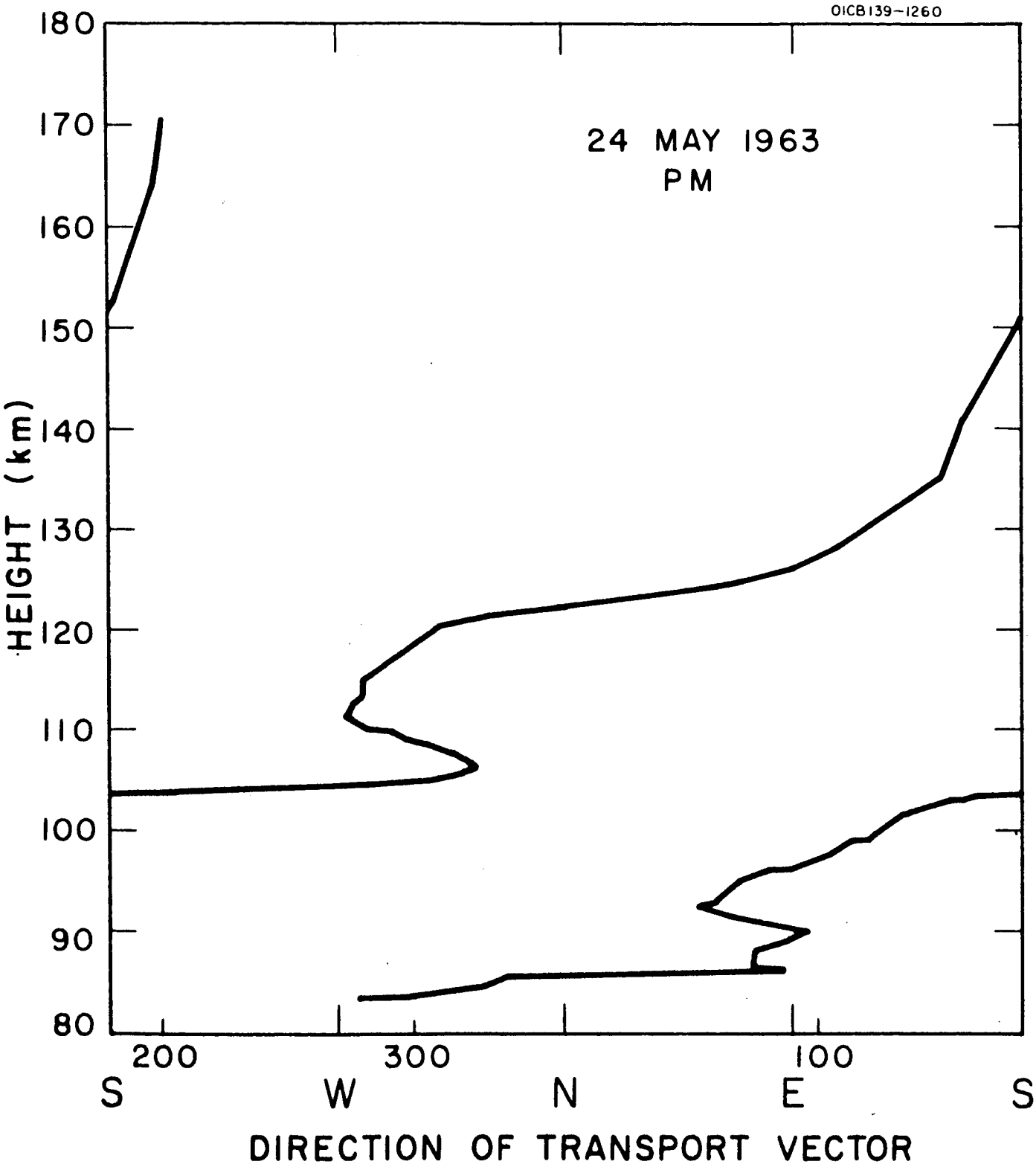

Figure 11. Direction of transport vector as a function of height for evening twilight of 24 May 1963 at Wallops.

The wind structures for the successive evenings at Wallops Island have some similarities, but greater differences. Below about 130 km, both patterns have numerous large shear regions, but the altitudes and relative magnitudes of these vary. The greatest difference is in the direction profile, which shows almost two complete 360^{o} rotations over the measured altitude on 25 May, but a reversal of direction on 24 May. Above 140 km, the winds are toward the southern hemisphere as has frequently been observed at Wallops.

The Churchill flights were the first to be made at that location. The winds from the first evening firing and the following morning are separated by only about four hours time difference and clearly show the changes in wind structure which occurred during this period. The most prominent feature of both of these plots is the high wind speeds at the high altitudes. Beginning at about 110 km, the speed continually increased with height until it reached a maximum speed of 220 meters/sec at 160 km for the evening twilight. During the following morning twilight, the speed increase with height was greater, reaching a value of 190 meters/sec at 125 km. This is a very different wind pattern than has been observed at Wallops Island. Similar structure at higher altitudes is sometimes observed at Wallops, but the speeds are much less and the pattern of increasing speed with altitude usually starts above 140 km, never as low as 110 km. On the following evening twilight at Churchill, the high speed upper winds had generally reduced to less than half of their previous value and a sharp shear had developed at

100 km. This latter pattern is not appreciably different from some previously obtained at Wallops Island.

The directional profile for the Churchill winds did not change greatly throughout the period. The wind direction was to the north only in the region 100-120 km. The upper winds are all toward the southern hemisphere as usually observed at Wallops Island.

Considerable effort has been applied to analysis of all of the Wallops Island data. At the present time, winds have been obtained from twenty-two different trails at Wallops. A preliminary analysis of this data was presented in the final report on contract NASw-396.[4] It was shown that the Wallops data and data from Sardinia fit a systematic closed figure at certain altitudes. A more detailed analysis of this representation has been made and a model of wind structure for the altitude range 85 to 135 km is proposed. The winds at any altitude are considered to contain a prevailing component and cyclic component with periods of 24-hours, 12-hours, and 8-hours. Values of the magnitude and relative phases of these components have been determined. The large irregularities observed in the winds are attributed to irregularities in phase of the resultant wind. A technical report entitled "An Experimentally Determined Model for the Periodic Character of Winds from 85 to 135 km," has been prepared which gives a detailed account of this analysis. The reader is referred to that report for the details.[8] A brief summary and discussion of the major results will be given here.

The key result, based on twenty-eight trails that have been measured since 1959, is that the wind vectors at any fixed height in the range 85 to 135 km trace out a closed curve consisting of three main loops. That such a curve can be drawn for a particular set of twenty-eight points is not especially significant. That the same kind of curve can be drawn for many sets of data points corresponding to a large number of fixed levels between 85 and 135 km, and that the characteristics of the curve change smoothly with height adds greatly to the significance of the result. Finally, when the empirical curves are fitted by a mathematical formula based on physical considerations, and the parameters that describe them are found to vary with height in a strikingly regular way, there seems to be little choice but to regard the patterns as significant. Nevertheless, our present conclusions should be regarded as tentative until enough new data have been gathered to afford a crucial test.

The fact that the horizontal wind patterns are closed curves suggests periodic motion. The three loops suggest a fundamental frequency and two overtones. Presumably, the fundamental frequency corresponds to a period of 24 hours and the two overtones to 12-hour and 8-hour components. A simple periodic oscillation is represented by an ellipse. Each cartesian component of the wind vector varies harmonically and the tip of the vector traverses the circumference of the ellipse in a time equal to the period of the oscillation. If several periodic components are present, the composite oscillation is described by a figure that

results from adding up the individual wind vectors at corresponding instants of time. In the case at hand, a figure with three main loops results. The form of the observed figures shows that the 8-hour component has the largest amplitude. The amplitude of the 12-hour component is about half that of the 8-hour component, while that of the 24-hour component is about half that of the 12-hour component. There is also a small prevailing component whose value is consistent with the much more accurate radio-echo determinations of the same quantity.

In the mathematical models, circular rather than elliptical loops were used for the individual periodic components. Actually, some evidence for ellipticity of the loops can be found in the data figures, but the additional complexity that would result from using elliptical loops offsets the gain in accuracy. When more data become available, a more refined analysis may become worthwhile.

The present analysis represents the resultant wind as follows:

$$W = W_o e^{i\alpha_o} + W_1 e^{i(\omega t + \alpha_1)} + W_2 e^{i(2\omega t + \alpha_2)} + W_3 e^{i(3\omega t + \alpha_3)}$$

The W's are the magnitude of the prevailing and cyclic components, and the α's are the relative phases. The values of the magnitudes of the components as determined from mathematical analysis of the data figures, are shown in Figure 12. It should be noted that the actual values of α_1, α_2, and α_3 cannot be determined uniquely without knowledge of a zero time. However, the relative phase of one component with respect

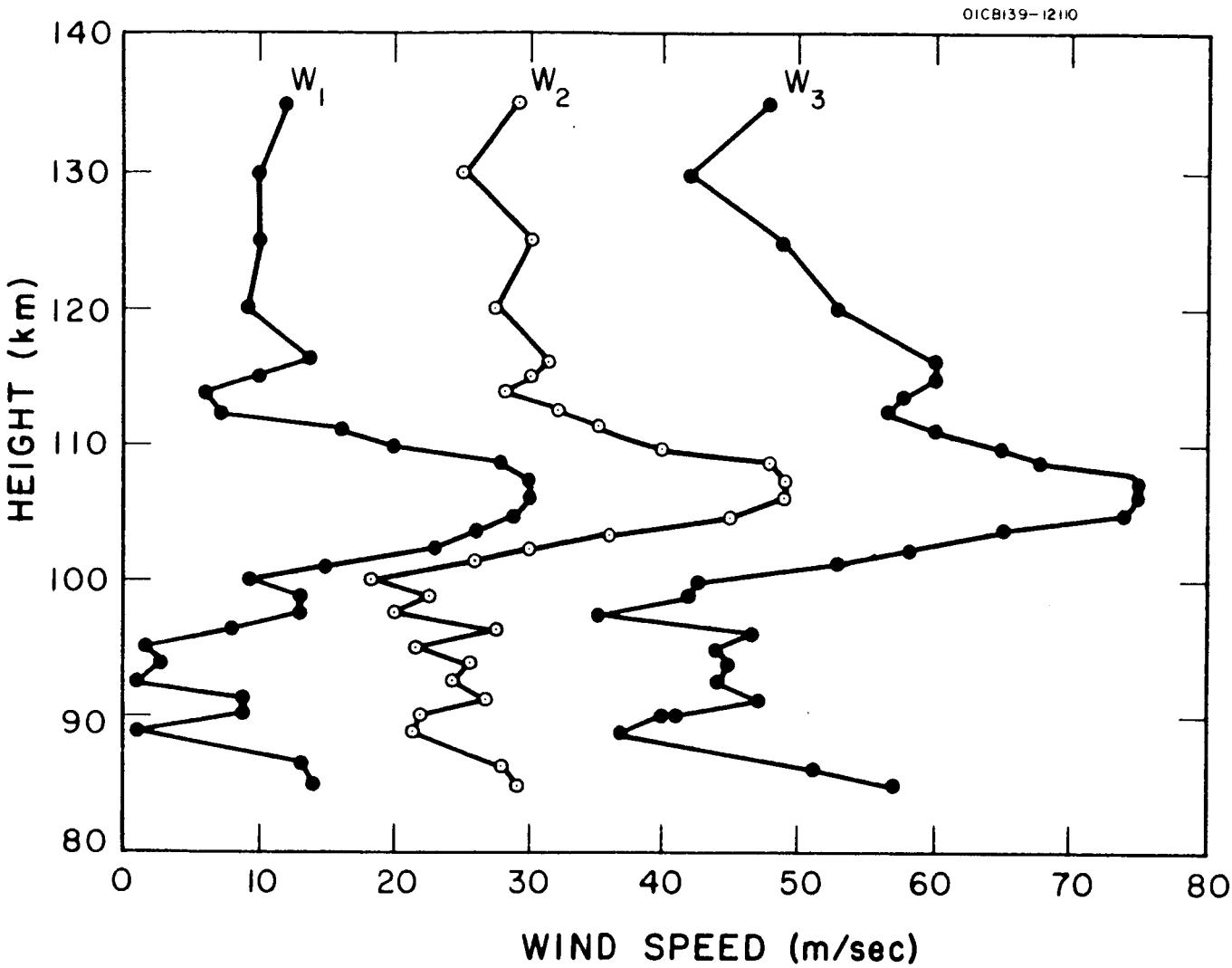

Figure 12. Observed values of W_1, W_2, and W_3 as a function of height.

to the others may be uniquely determined for two of the components. This phase information allows determination of permissible values of the α's. Two such combinations are shown in Figure 13. The magnitude and direction of the prevailing component is given in Figures 14 and 15.

All the empirical wind patterns can be accurately represented by theoretical curves. The derived amplitudes and phases of the periodic components vary with height in a simple and regular way. Especially notable is the tendency for phase changes to be concentrated in narrow layers and for these changes to amount to 180^{o} or 360^{o}. Since the phases result from detailed analysis -- one cannot estimate them accurately simply by inspecting the figures -- this result affords convincing evidence that the mathematical representations have genuine physical significance.

Although the tip of the wind vector at a given height sweeps out a periodic pattern, the rate at which it does so is not consistent with periodic motion. If the winds were truly periodic, any given pair of points on the wind pattern would correspond to a definite increment of the local time and a given point would always correspond to the same local time. The observed local times do not conform to these rules. One can describe the situation mathematically by saying that the phase of the wind at any given height contains a large contribution that varies irregularly -- or at least in an unknown way -- with time. The variable part of the phase is common to all the components. If it were not, the

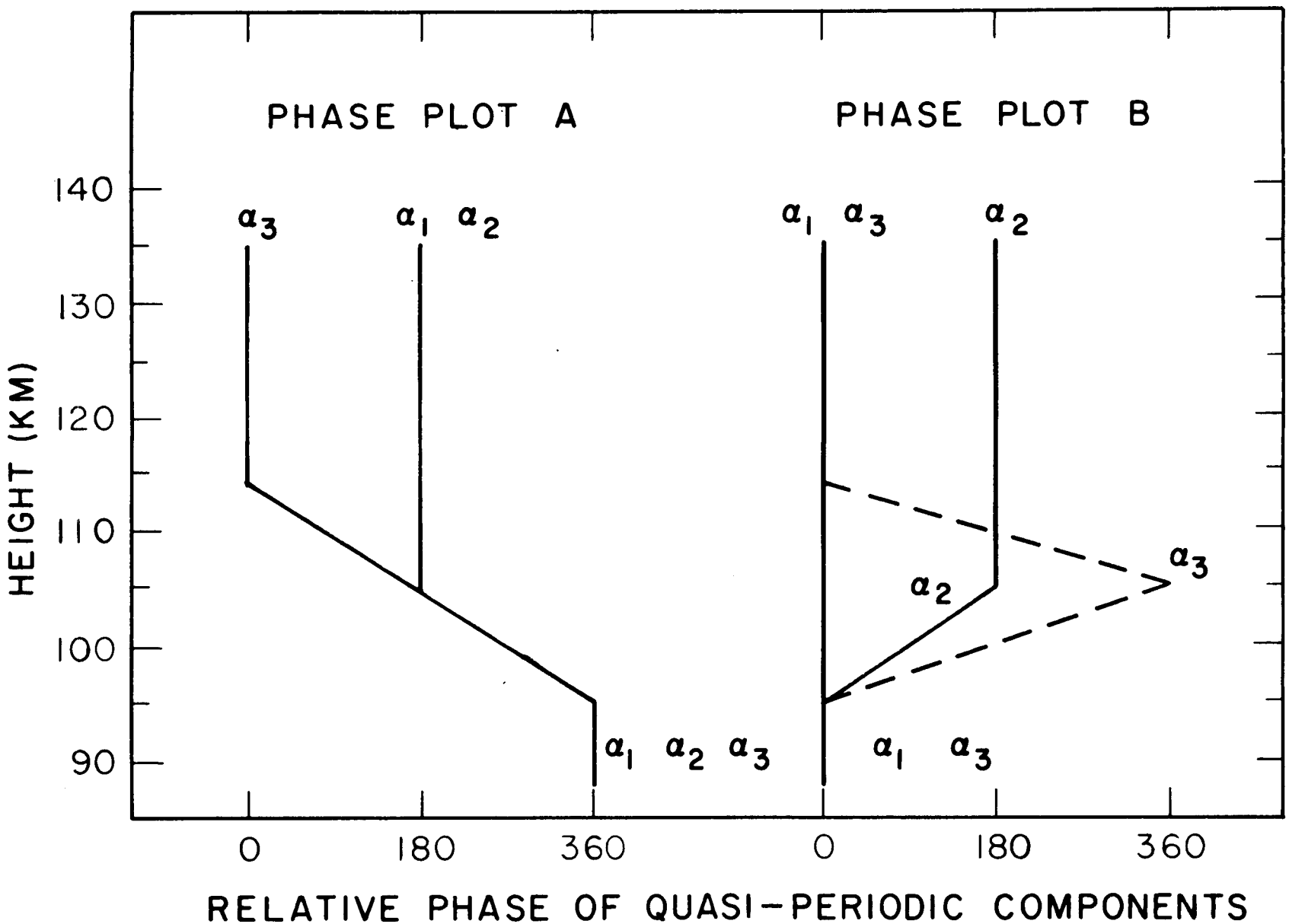

Figure 13. Two possible variations of the relative phase of quasi-periodic components with height.

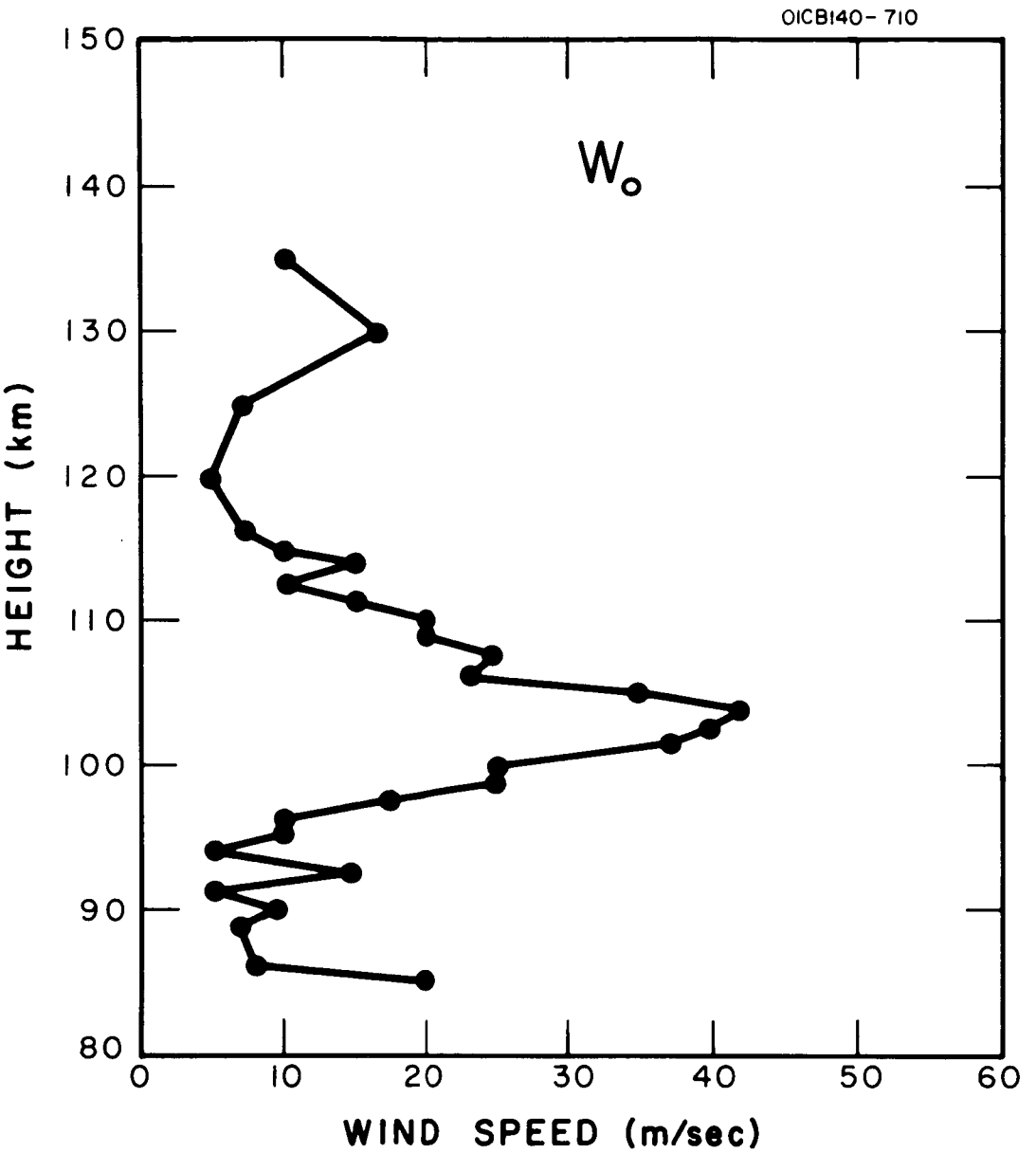

Figure 14. Observed values of W_o as a function of height.

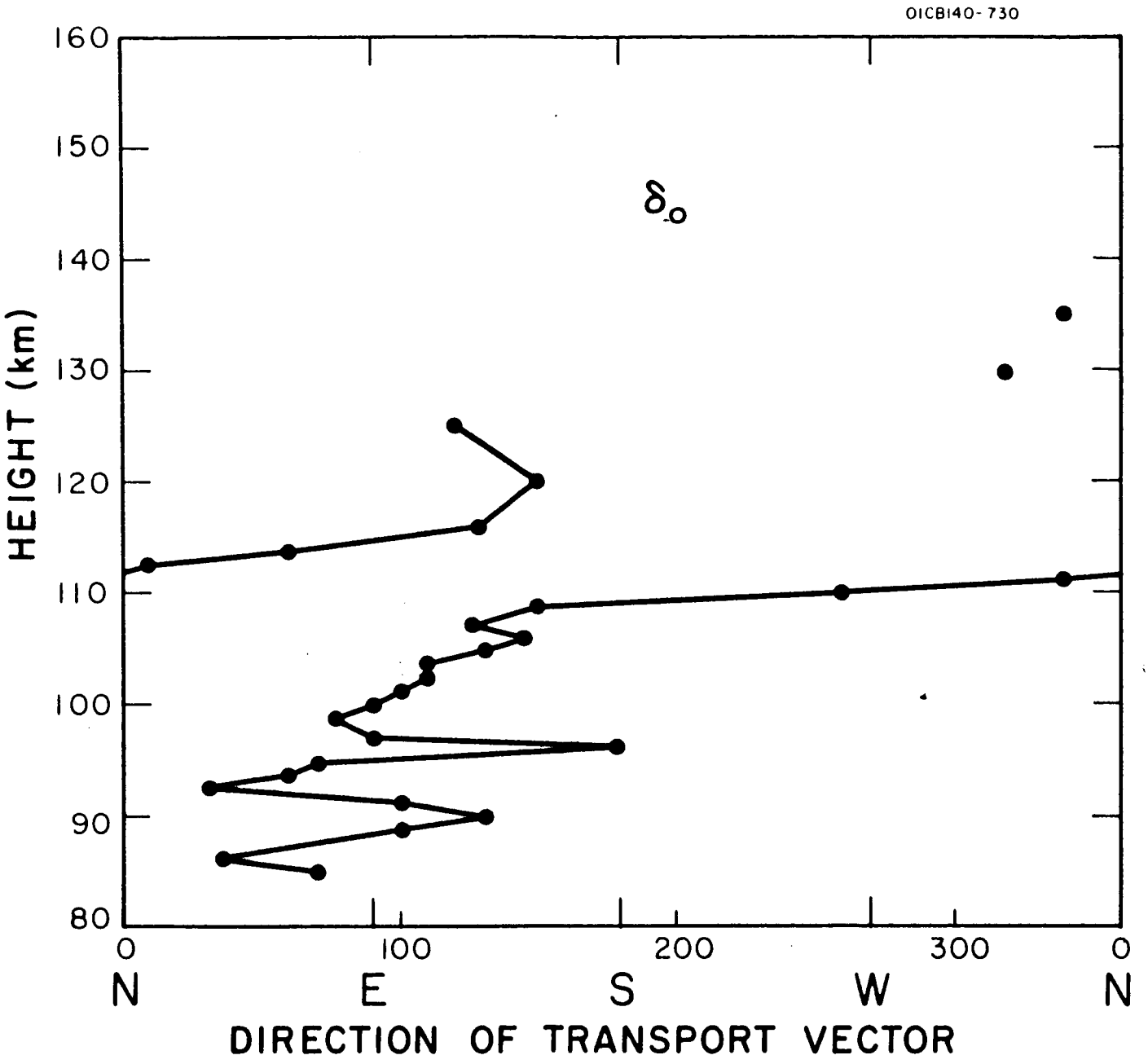

Figure 15. Observed values of δ_o as a function of height.

tip of the wind vector would not trace a closed loop, but would wander all over a two-dimensional region. Thus the cyclic components are best described as quasi-periodic.

The available data are sufficiently numerous to show marked seasonal effects if they were present, but no such effects have so far been isolated.

The irregular contribution to the phase of the wind vector is chiefly responsible for the fact that the amplitudes of the periodic components given by the present analysis are much larger than those derived from the radio-echo data. The irregular phase contribution is particularly effective in reducing the amplitude of the 8-hour component because discrepancies between actual and "predicted" local times are normally of the order of several hours. It is worth emphasizing that no contraduction exists between the results of the present analysis and the results of the radio-echo analysis. However, the physical pictures suggested by the two analyses are quite different.

The picture of wind structure that emerges from the present analysis does not fit into the conventional theory of forced atmospheric oscillations. Even if the theory were modified to allow for the effects of nonlinearity above 90 km, it would not account for the variability of the total phase. Thus if the picture is confirmed by future experimental studies, the theory will need to be modified in a fundamental way. Some preliminary work on these lines has already been undertaken.

SECTION 4

DIFFUSION DATA

Diffusion coefficients have been determined from most of the vapor trails obtained at Wallops Island since 1959 and the three trails from Fort Churchill. The amount of reliable data obtained from each trail varies greatly due to many factors. The best method of analysis depends on careful densitometry of trail image in which both the sky background and the optically dense center of the trail are recorded on the linear portion of the E and H curve of the film. For most films, this condition requires the use of most of the linear portion of the curve, and conditions such as haze and background variations reduce the reliability of the data. Also, densitometry of some regions of the trail is prevented by strong wind shears or overlap in the direction of view. Atmospheric clouds also prevent useful densitometry even though the trail is often visible through them and accurate winds may be determined. These factors greatly limit the data at altitudes above 180 km, where the diffusion rates are so fast that the cloud center remains optically dense for only a few minutes and the useful observing time is thus short. The error in exact altitude determination is also increased for trails

of greater widths, causing a wider spread in the experimentally determined points. Some of the data also contains uncertainties which may be due to the presence of some lithium light on the sodium trail negatives. The long wavelength cutoff of panchromatic film is used to reject the lithium light, but some of the new films have greater red response and sometimes large amounts of lithium were used. This effect has not yet been completely evaluated and that data is not included in the averages.

A complete description of the analytical methods used in data reduction has been given previously[2,9]. The total data to date is presented and discussed in this report. The data is tabulated by date and altitude in Table 2. The amount of data decreases at higher altitudes, and values from each trail may have been obtained from several different observing sites because of the previously mentioned restrictions.

The diffusion coefficient for a minor gas in the earth's atmosphere may be represented as follows:

$$D = Cn^{-1}\left(\frac{1}{m} + \frac{1}{mi}\right)^{1/2} T^{1/2}$$

where D is the coefficient for the diffusion of the gas of molecular weight mi into the ambient of mean molecular weight, m, and number density, n. T is the absolute temperature and C (although it depends on the effective cross section of the gases) is essentially constant for a particular vapor. The 1962 ARDC Standard Atmosphere proposes an

TABLE 2

DIFFUSION COEFFICIENT - WALLOPS

Date	Height(km)	D(cm^2/sec)
19 April 61	105	2.02×10^6
	107	3.00
(3 sec)	110	3.64
	112	9.88
	115	1.09×10^7
	120	5.24
	125	5.59
	130	1.02×10^8
	140	1.99
	150	2.57
	155	2.82
20 April 61	120	4.11×10^7
	130	8.02
(3 sec)	135	1.35×10^8
	150	2.69
	155	3.58
	170	6.52
21 April 61	100	2.07×10^6
	118	1.72×10^7
(3 sec)	120	4.01
	125	4.93
	130	8.16
	140	2.13×10^8
	150	3.35
	160	3.99
16 Sept 61	107	3.55×10^6
	110	5.85
(7 sec)	114	8.09
	115	1.07×10^7
	145	2.24×10^8
	160	5.53
	170	5.54
	180	8.04
	190	8.64
	200	1.09×10^9
17 Sept 61	100	2.51×10^6
	104	3.92
(7 sec)	107	3.22
	112	6.86
	116	1.51×10^7
	120	3.42
	130	9.10
	140	1.69×10^8
	150	2.80
	160	4.49
	170	5.99
1 March 62	106	3.42×10^6
	110	6.86
(8 sec)	115	1.26×10^7
	120	2.29
	125	4.19
	130	6.94

TABLE 2 (continued)

Date	Height(km)	D(cm^2/sec)	Date	Height(km)	D(cm^2/sec)
2 March 62	104	1.04×10^6	23 May 63	111	5.55×10^6
	106	2.36		115	1.13×10^7
(8 sec)	108	3.96	(7 sec)	120	2.36
	110	6.51		125	4.24
	112	6.17		150	3.40×10^8
	115	9.18		175	7.37
	125	3.18×10^7			
23 March 62	106	5.86×10^6			
	114	1.05×10^7			
(7 sec)	120	2.08			
	122	2.95			
	132	4.16			
27 March 62	105	2.98×10^6			
	107	3.83			
(3 sec)	110	3.98			
	113	6.22			
	119	1.32×10^7			
30 Nov. 62	106	2.70×10^6			
	110	5.22			
(7 sec)	114	7.81			
	120	4.71×10^7			
	130	1.09×10^8			
	140	2.08			
	150	2.85			
	160	5.88			
21 Feb 63	110	8.64×10^6			
	115	1.32×10^7			
(7 sec)	130	1.08×10^8			
	140	2.02			

TABLE 2 (continued)

DIFFUSION COEFFICIENT - CHURCHILL

Date	Height (km)	D (cm^2/sec)
21 May 63	106	3.69×10^6
PM	110	9.90
	117	2.72×10^7
	124	3.43
22 May 63	108	5.86×10^6
AM	112	8.71
	116	1.33×10^7
	118	2.06
	124	3.84
22 May 63	112	1.27×10^7
PM	114	1.57
	120	2.81
	127	7.55
	136	1.11×10^8
DIFFUSION COEFFICIENTS ABOVE 200 KM		
13 Sept 61	202	1.18×10^9
AM	211	1.76
	218	1.79
	231	3.50
	242	4.37
	260	4.59
	277	9.00×10^9
	410	2.77×10^{11}
13 Sept 61	410	2.16×10^{11}
PM		
10 Dec 60	370	3.8×10^{10}
PM		

approximately linear variation of m in the range 100 to 200 km. The values at those altitudes being about 29 and 25.5 respectively. Thus the value of the reduced mass, (1/m + 1/mi), has very little variation over that height range, since mi is 7 for lithium and 23 for sodium. The ratio of the diffusion coefficients, DLi/DNa, at a particular height in this altitude range is almost 1.7 if an average value of m and appropriate values of the cross section are used. The experimental measures show approximately this value, but the number of measurements of lithium is still small and thus the averaged value contains relatively large errors.

If the variation in the reduced mass is neglected over the altitude involved, the height variation of the coefficients may be written:

$$D = D_o \frac{\sqrt{T/T_o}}{n/n_o}$$

where D_o is the value of the coefficient at a reference height at which $T = T_o$, and $n = n_o$.

The resulting height variation of D as obtained from the various proposed ARDC Standard Atmospheres are shown in Figure 16 along with the averaged experimental curve obtained at Wallops Island for sodium. The values of T_o and n_o were taken as the ground value from the 1962 Standard Atmosphere. The value of D_o is taken equal to 0.2 cm^2/sec. Normalization of the various curves at some point in the region of diffusion measurements causes a distortion of the relative curves due to the changing

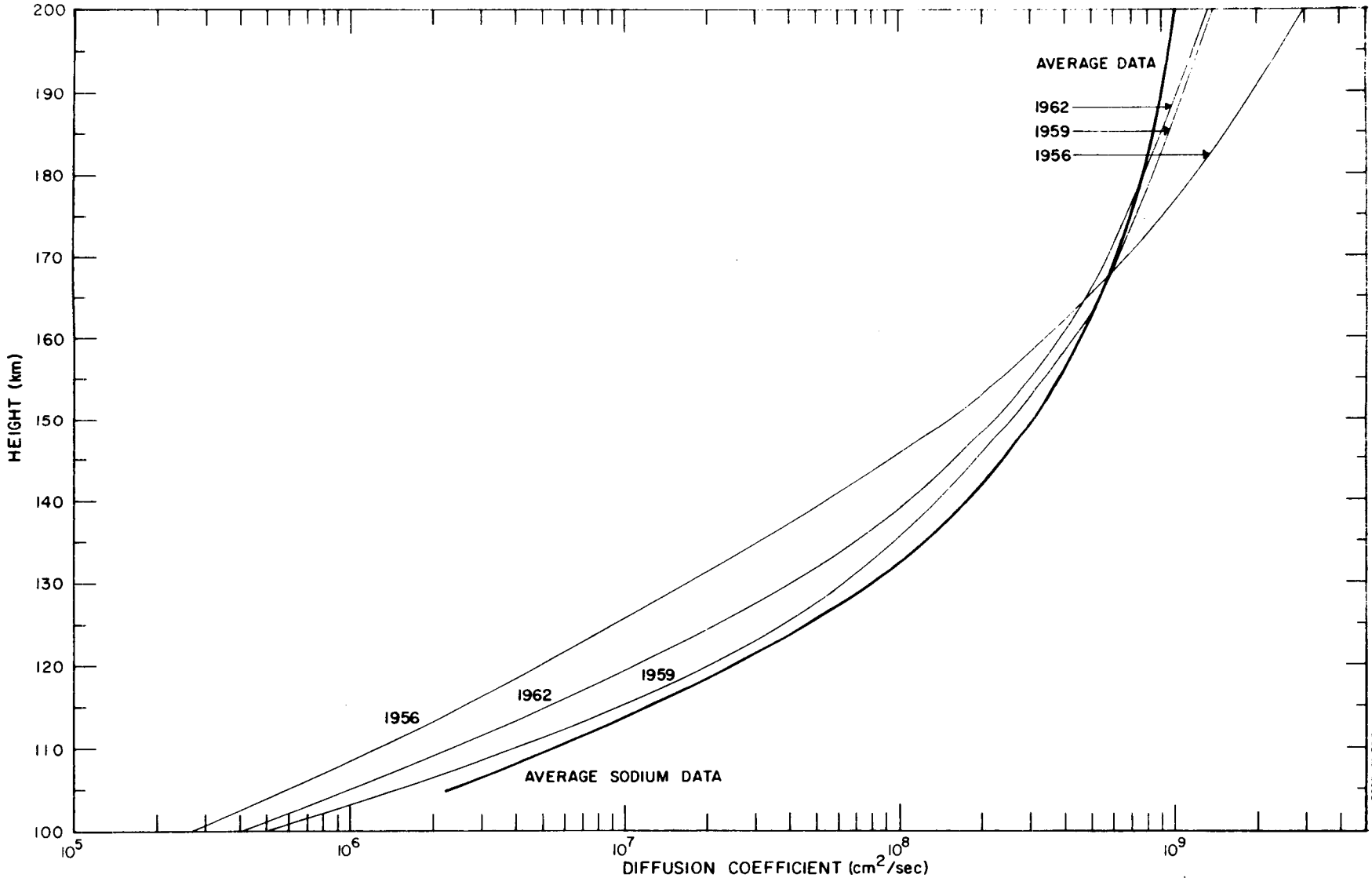

Figure 16. Height variation of the diffusion coefficient from 100 to 200 km determined from average sodium data, and compared to that obtained from the ARDC Standard Armosphere of 1956, 1959, and 1962.

slopes. The measured diffusion coefficients confirm the relative accuracy of the most recent standards. However, there is some inconsistency between the measurements and the standards. If the variations in mean molecular weight are neglected, the quantity $Dn\sqrt{T}$ should be constant with height. This quantity, composed of the measured diffusion coefficients and other values from the 1962 standard, is plotted as a function of height in Figure 17. The variation from a constant value is a factor of 3 over the average 100 to 200 km altitude range. Thus the diffusion coefficients indicate a smaller height gradient of the factor $n\sqrt{T}$ than is shown by the Standard Atmosphere.

The averaged curve for diffusion coefficients obtained at Fort Churchill is shown in Figure 18. It should be remembered that this curve is constructed from a very small amount of data. Figure 19 shows previous measurements of diffusion at higher altitudes compared to the Standard Atmosphere.

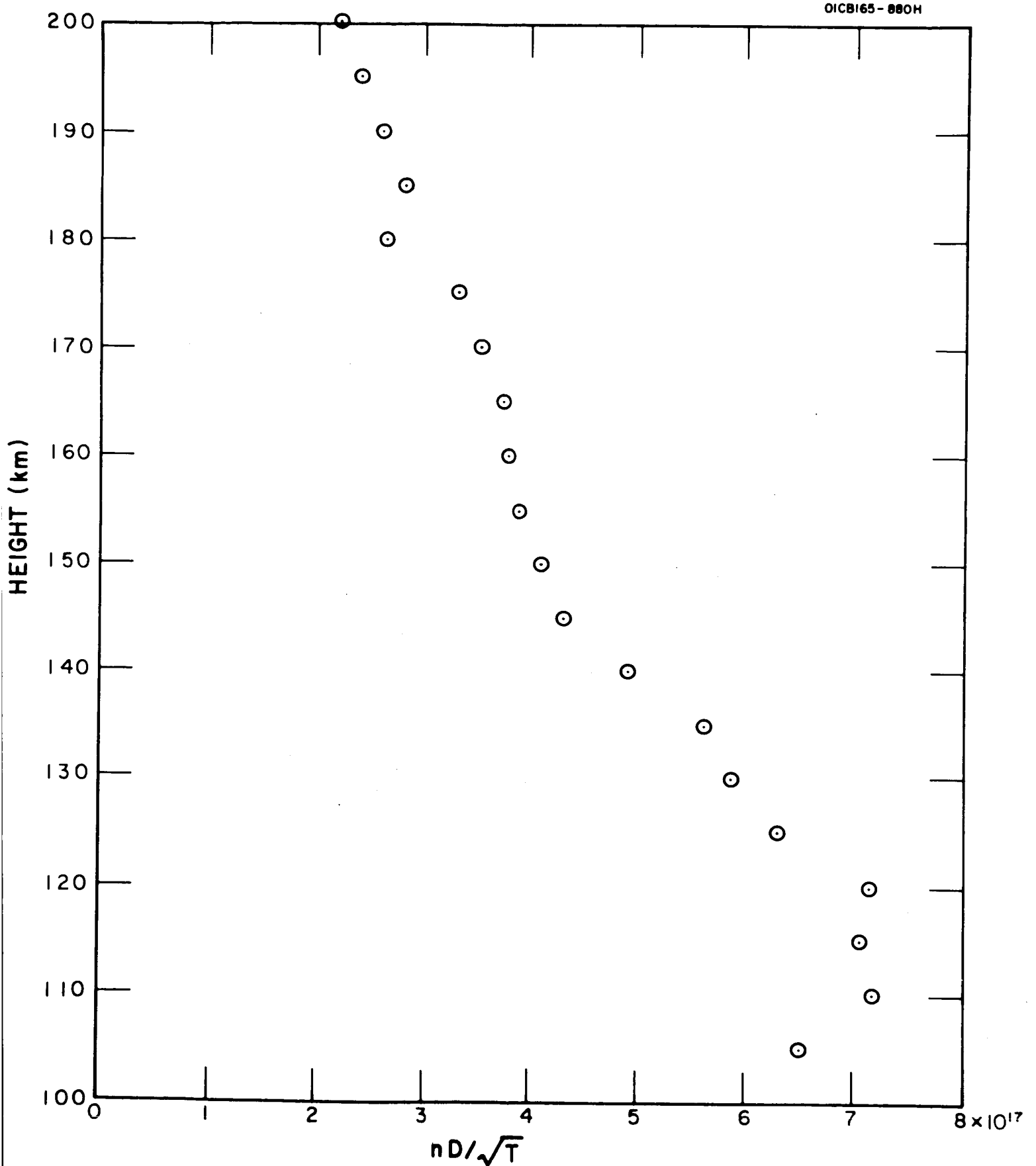

Figure 17. Height variation of $nD/\sqrt{T}$.

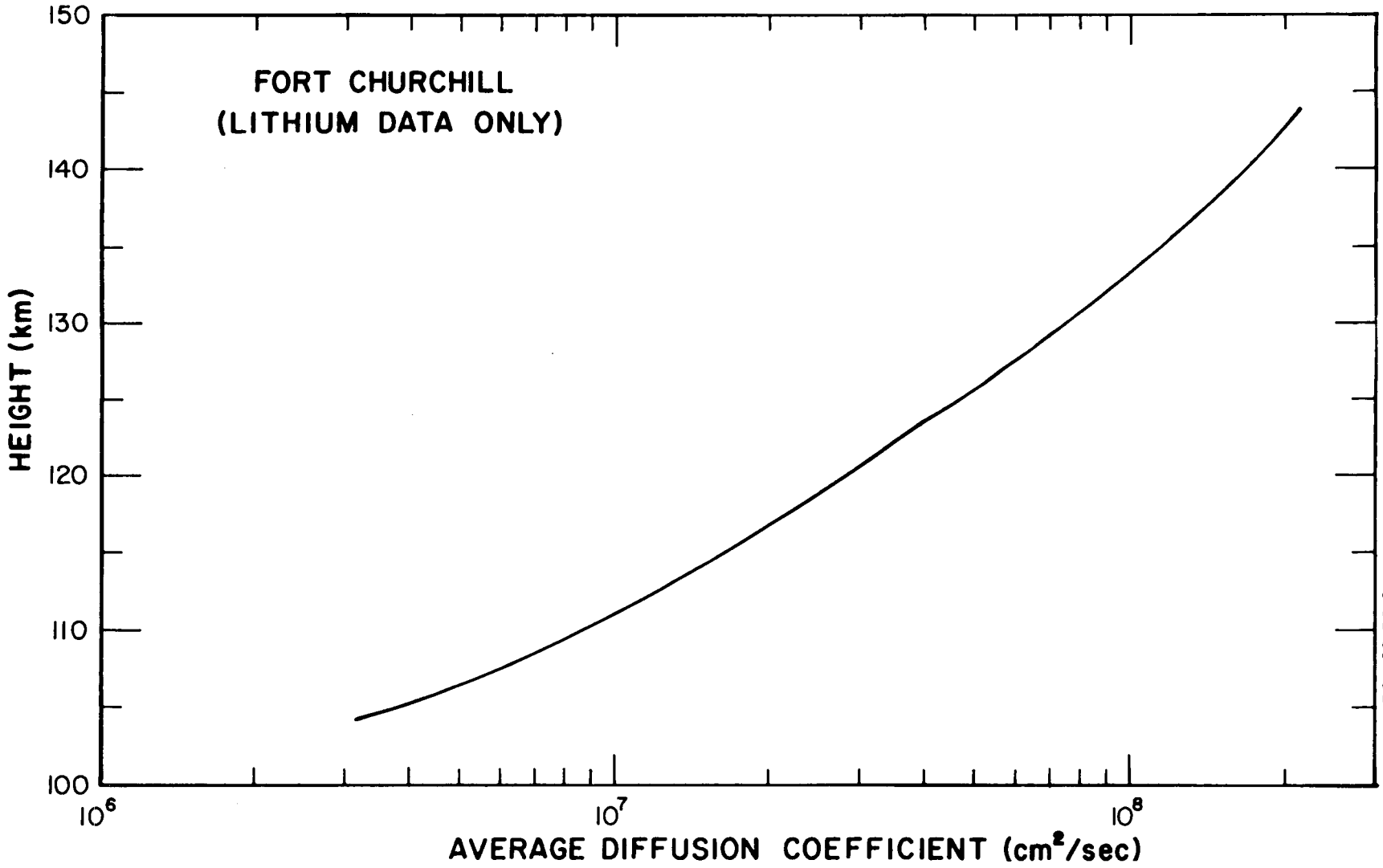

Figure 18. Height variation of the diffusion coefficient determined from average lithium data obtained at Fort Churchill.

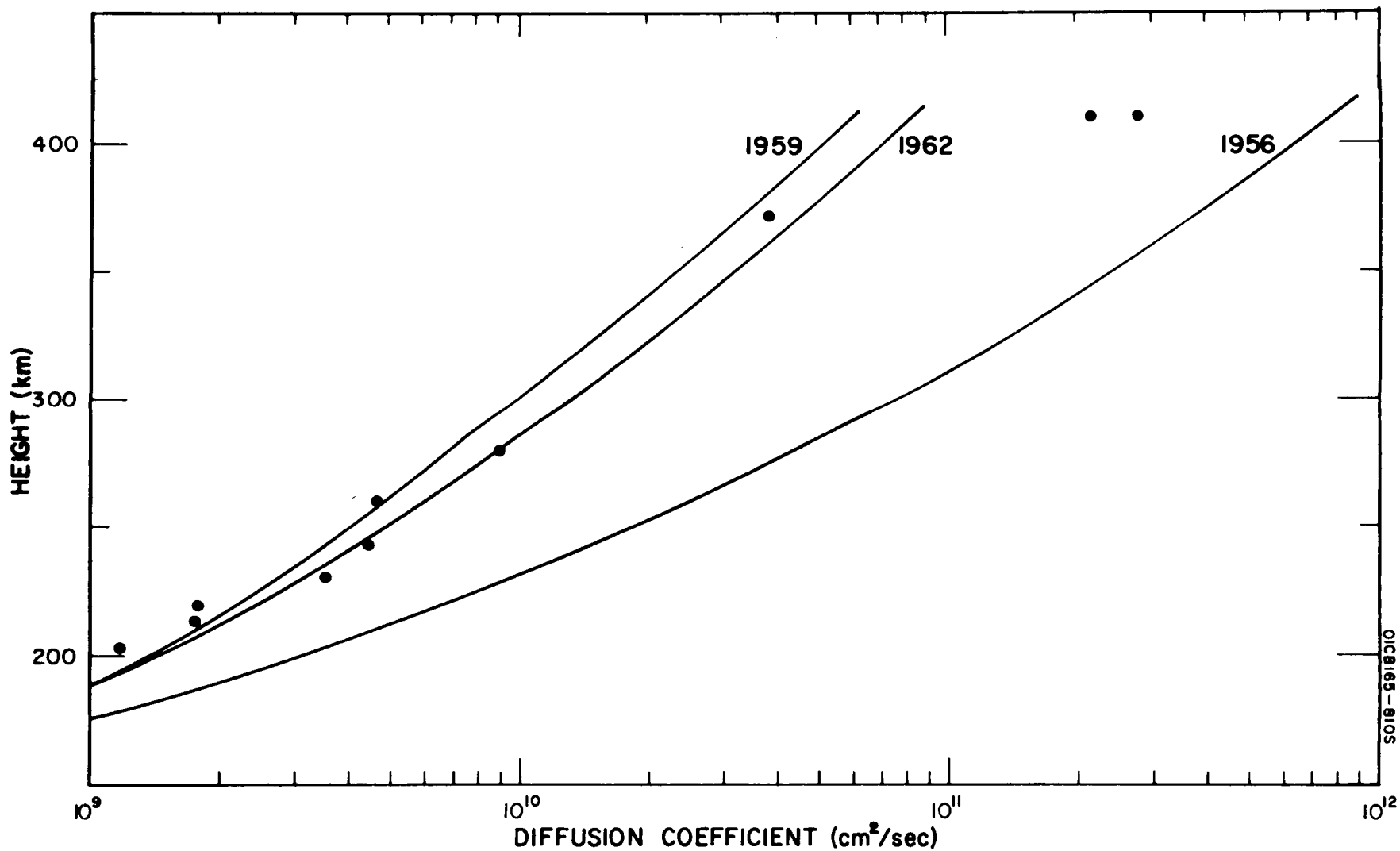

Figure 19. Height variation of the diffusion coefficient from 200 to 400 km determined from sodium data, and compared to that obtained from the ARDC Standard Atmosphere of 1956, 1959, and 1962.

SECTION 5

TURBULENCE

Above a height of 110 km, the sodium trails nearly always appear smooth and diffusion coefficients determined from the expansion rate are in good accord with the theory of molecular diffusion. Below this height, the trails generally are not smooth in appearance and this irregular structure together with an expansion rate greater than is expected from molecular diffusion alone has raised the question of the existance of turbulence in the atmosphere. This question was discussed in GCA Technical Report No. 62-12-N entitled "On the Question of Turbulence in the Upper Atmosphere."[10] In this report, the mathematical representation of hydrodynamic turbulence was discussed. The difficulties of a general solution to the problem were indicated and the results of the most developed theories were discussed. It is apparent that a complete statistical theory of turbulence which can be directly applied to the upper atmosphere does not exist at the present. However, the most widely known theory was originally developed by Kolmogoroff and has since been modified by many authors. The basic concept is that, at high Reynolds numbers all turbulent motion has the same sort of small scale structure which is isotropic and statistically uniform even though the

mean flow may vary widely. A turbulent flow is considered to be composed of a spectrum of eddies having effective wavelengths which vary from those characteristic of the mean flow down to a lower limit where energy is absorbed into the random heat motion of the molecules by viscosity. Energy from the mean flow is transferred to the larger eddies and then on down the spectrum until it is converted into heat. On this basis, Kolmogoroff formulated two similarity hypotheses,

(1) The statistical characteristics of the turbulent motion depend only on the mean energy dissipation per unit mass of fluid and on viscosity.

(2) The statistical characteristics of the larger eddies depend only upon the rate of energy dissipation.

From these hypotheses, one can derive certain predictions concerning the flow. The expansion rate can be shown to be:

(1) For small times: $< r^2 > - < r_o^2 > \sim T^2$

(2) For intermediate times: $< r^2 > \sim T^3$

Other approaches to the problem have predicted expansion rates which are governed by even higher valued functions of time. The reader is referred to the previous report for details of the theories.

In the referenced report, attempts were made to interpret the growth of the irregular portions of the trails as turbulence in the atmosphere. These attempts were not conclusive because of certain errors

inherent in the analytical method. Since that time, more data have become available and careful analysis has yielded definite growth rates in some regions of the irregular trail. Perhaps the most information was obtained in January 1964, at which time the appearance and growth of the trail were recorded with a camera having a 36" focal length. The enlarged image showed the initial appearance and growth of the trail irregularities. Photographs of this trail are shown in Figures 20 to 24. The successive photographs show that the trail irregularity has two distinct types of structure. Below about 100 km, the appearance may be described as "stringy," and above 100 km the structure which develops may be termed "globular." In both regions, the trail expands at a rate much faster than expected from molecular diffusion, and irregular structure develops rapidly. However, as is easily noted in the "globules," the individual shapes change very little even though the growth is rapid.

This appearance is typical of most of the vapor trails. However, all trails do not have as much developed "globular" structure. Table 3 is a summary of data on all of the trails from Wallops Island in which the occurrence or absence of the "globules" could be determined. It is seen that they occur in the region 100 to 110 km, and may be present in any part or nearly all of this region. The "stringy" type of irregularity is always below this altitude and appears in most trails. A fact worthy of note is that the presence of the globules is independent of the wind shear at that height. They are present with about equal frequency at times when the shear is near zero as in Figure 20, and at times of high

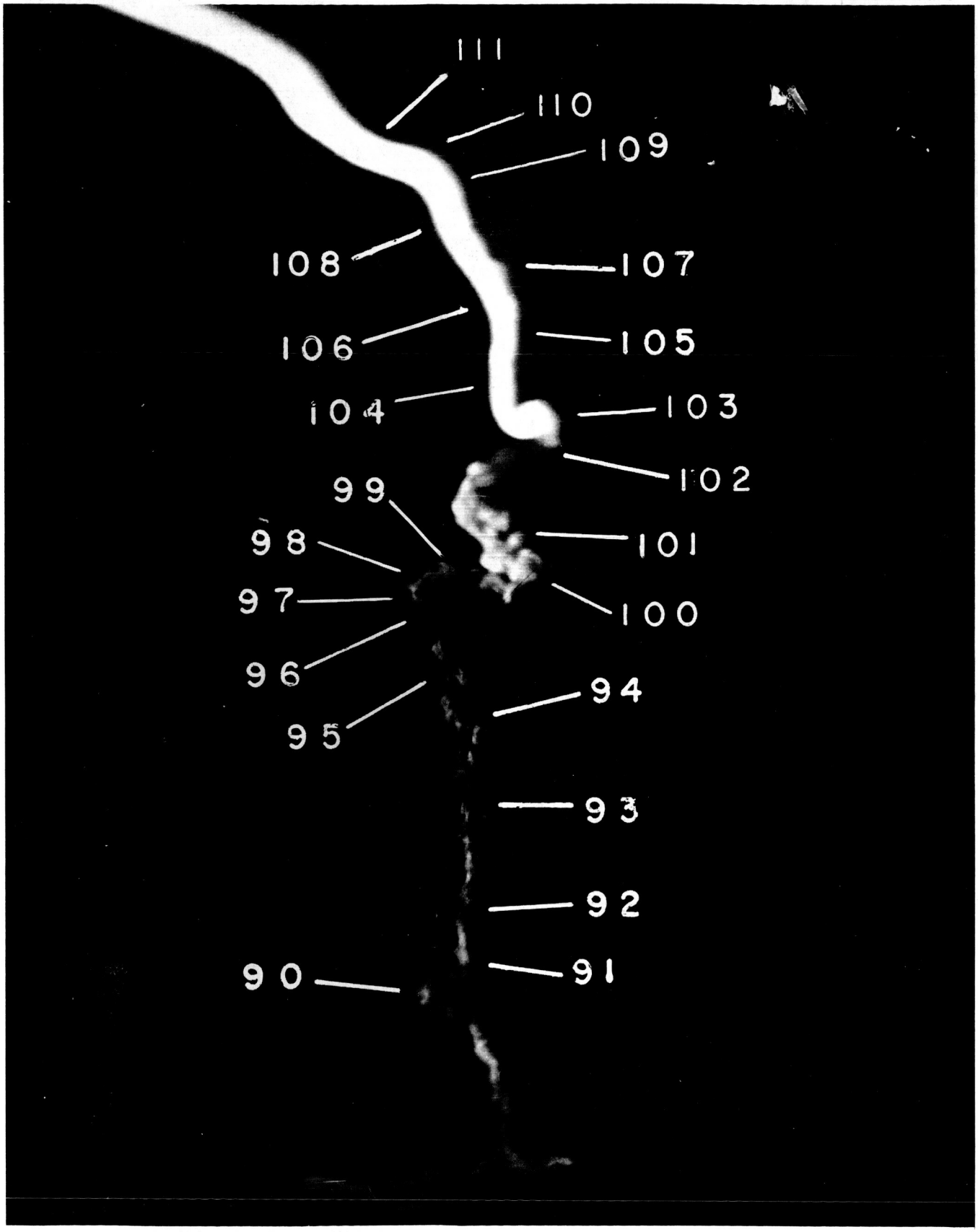

Figure 20. Photograph of vapor trail for 16 January 1964, morning twilight, from Dover at 122 seconds after launch.

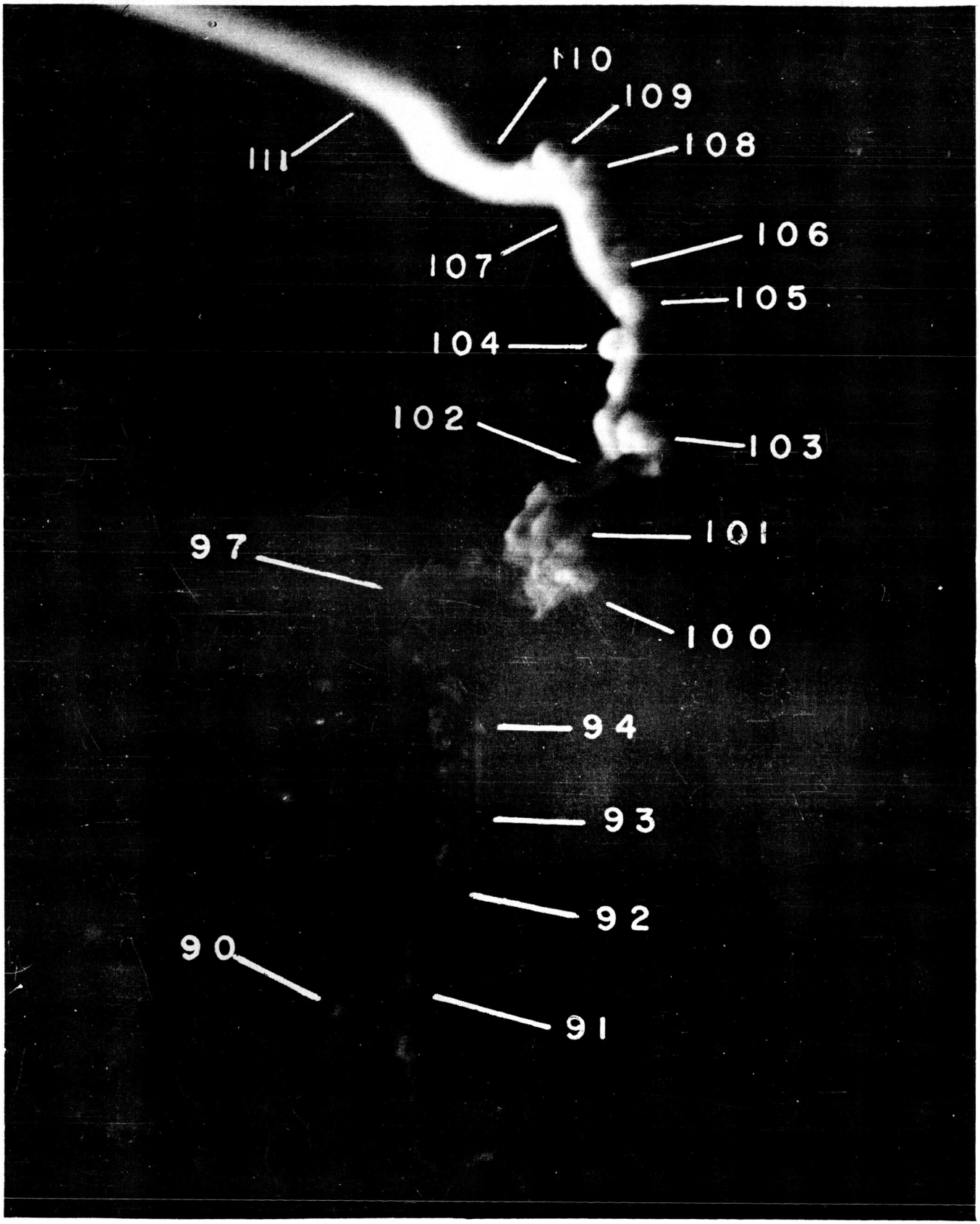

Figure 21. Photograph of vapor trail for 16 January 1964, morning twilight, from Dover at 152 seconds after launch.

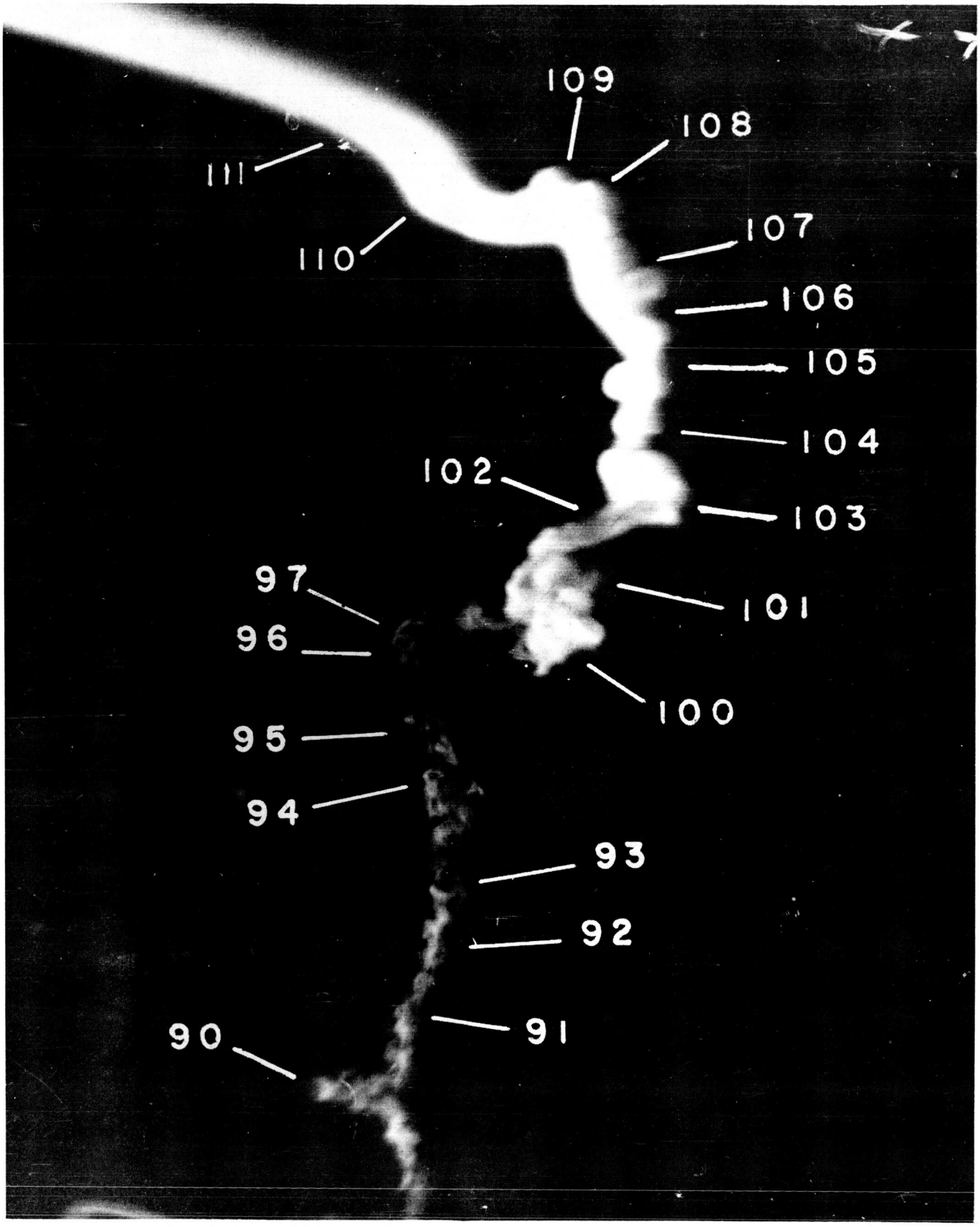

Figure 22. Photograph of vapor trail for 16 January 1964, morning twilight, from Dover at 153 seconds after launch.

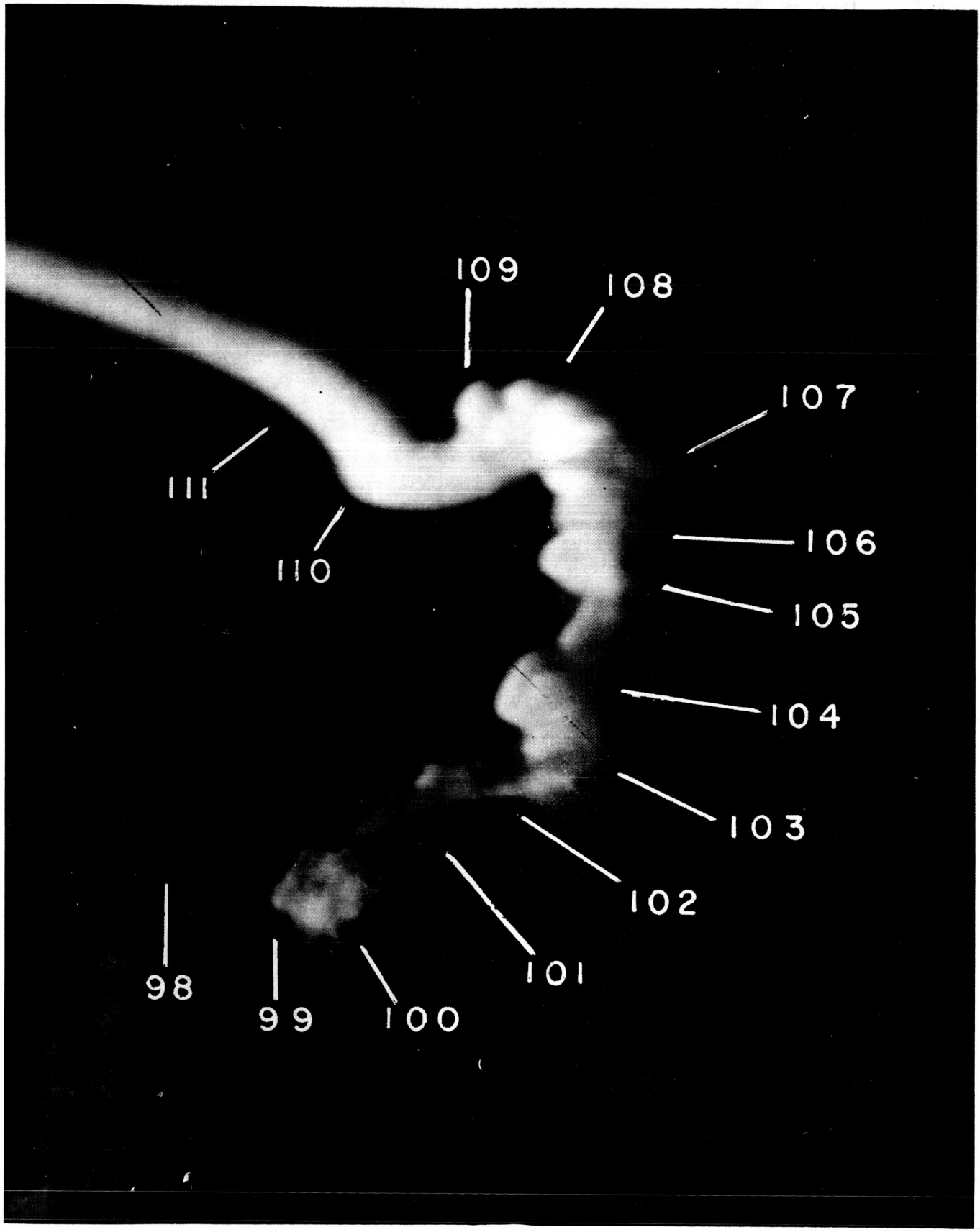

Figure 23. Photograph of vapor trail for 16 January 1964, morning twilight, from Dover at 182 seconds after launch.

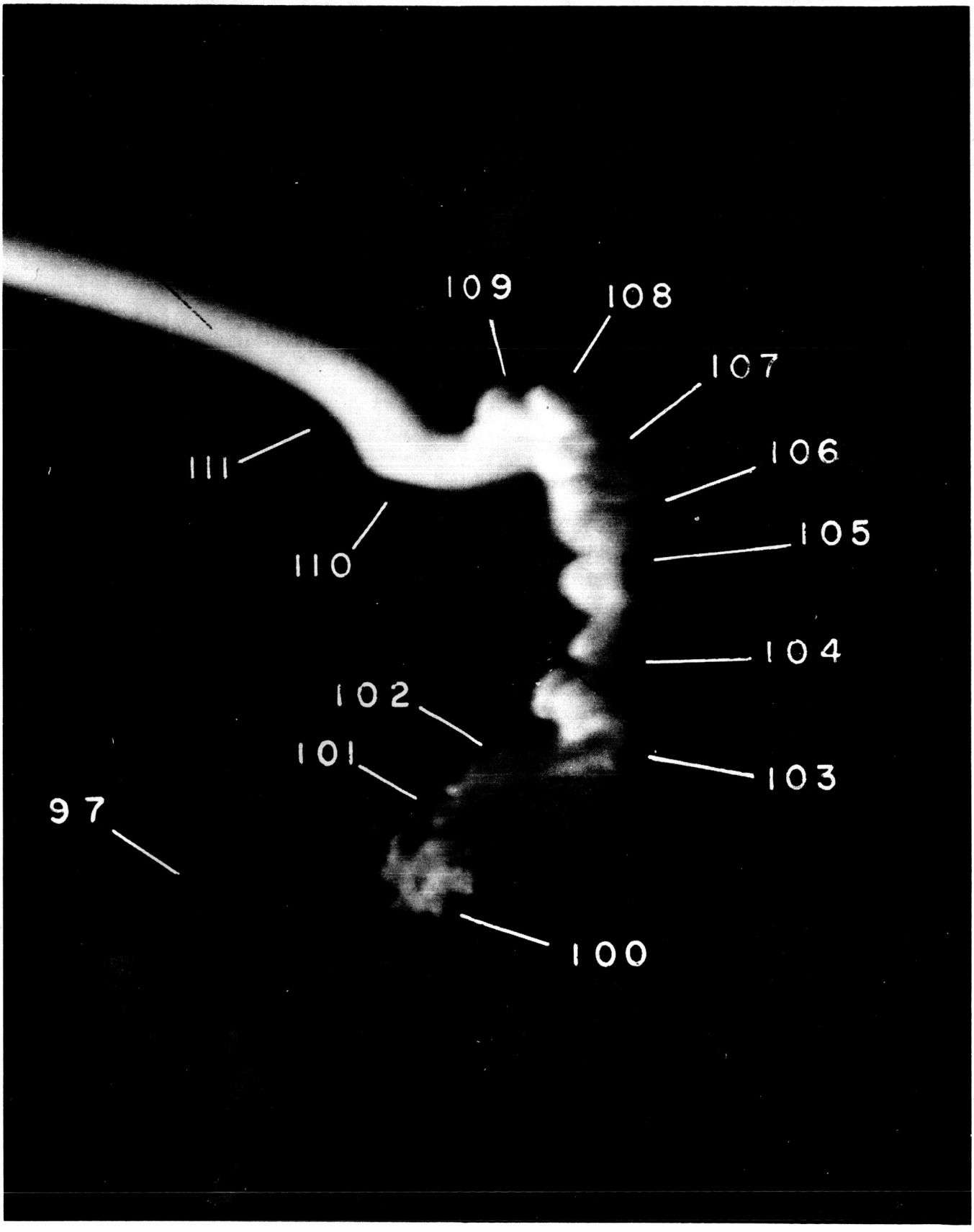

Figure 24. Photograph of vapor trail for 16 January 1964, morning twilight, from Dover at 212 seconds after launch.

TABLE 3

TURBULENCE

Twilight Period	Date	End of Turbulence	Change from Globules to Strings	Height Interval (km)	Shear	No Shear	Height for Plumes
PM	18 Nov 1959	93	---	0	---	---	---
PM	24 May 1960	111	107	4	x		107-111
		103	97	6		x	--
AM	9 Dec 1960	105	97	8	x		105
AM	19 April 1961	104	100	4	x		104
PM	20 April 1961	106	96	10	x		106
AM	21 April 1961	108	102	6	x		102-108
PM	16 Sept 1961	108	104	4		x	---
AM	17 Sept 1961	111	100	10	x		102
PM	1 March 1962	107	96	11	x		107
AM	2 March 1962	104	97	7		x	---
PM	23 March 1962	106	102	4	x		106
PM	27 March 1962	107	98	7		x	---
AM	17 April 1962	107	103	4		x	---
PM	6 June 1962	101	---	0	---	---	---
AM	7 Nov 1962	109	101	8	x		108
AM	30 Nov 1962	102	---	0	x		102
PM	20 Feb 1963	111	109	2		x	---
		106	96	10	x		---
PM	21 Feb 1963	108	105	3	x		105-107
PM	21 May 1963	105	98	7	x		105
AM	22 May 1963	99	97	2		x	---
PM	22 May 1963	99	95	4		x	99
PM	23 May 1963	104	95	9		x	104
PM	24 May 1963	105	103	2	x		104
PM	15 Jan 1964	100	96	4	x		---
AM	16 Jan 1964	109	104	5		x	---
				TOTALS	15	10	15

shear as in Figure 25. When a shear is present, this initial, nearly spherical, shape of the globule is quickly distorted by the shear, and sometimes forms long plumes as shown in Figure 26. Only at times of low shear is the constancy of shape readily apparent even though the scale is changing rapidly. At these times the growth rate may be measured with high accuracy. Several such "globules" have been measured. Some of the growth rates are shown in Table 4 and in Figure 27. The radii of the globules are shown as a function of time. The increase in radius is seen to be linear with time, at a rate of from 3 to 5 m/sec. The rates appear to be independent of altitude but continue for as long as observation is possible on any trail. One of the trails at Ft. Churchill was observed for about 18 minutes. It is often possible to measure the growth of trails between expanding globules. The growth rate of these parts of the trail is the same as that of the globules. At altitudes below the globular region the growth is much more difficult to measure. The "stringy" portion generally has no symmetrically shaped parts and because of the greatly varying density across the width of the trail, uncertainties in the photographic recording are increased. However, some regions permit accurate measurement, and average measurements of total width have been made on several trails. The trail growth at these altitudes show the same time dependence as above but the rate is lower. Figure 28 shows the growth rate of non-globular parts of the trails.

Interpretation of these observations in terms of the present mathematical representation of hydrodynamic turbulence presents some serious

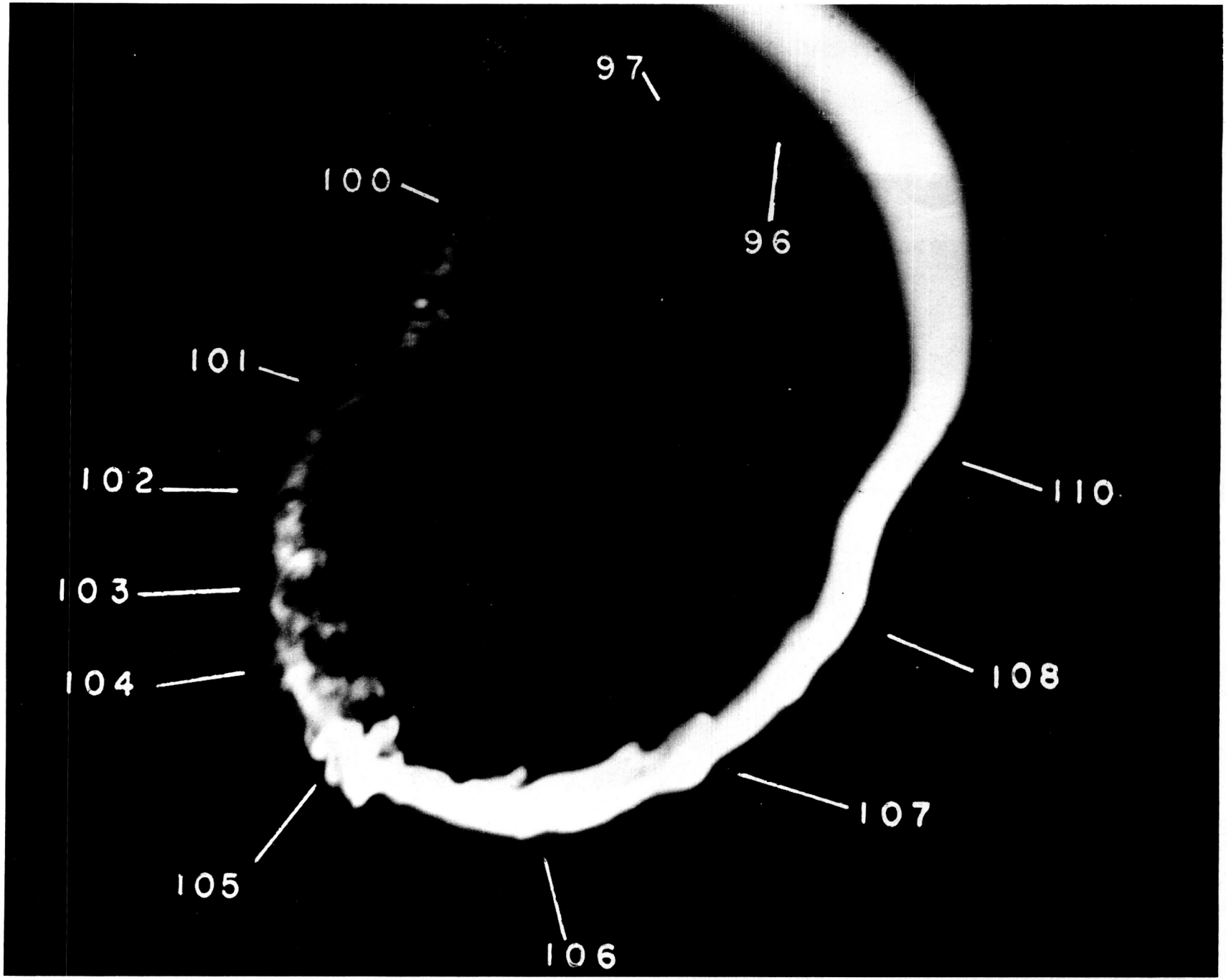

Figure 25. Photograph of vapor trail for 1 March 1962, evening twilight, from Dover at 360 seconds after launch.

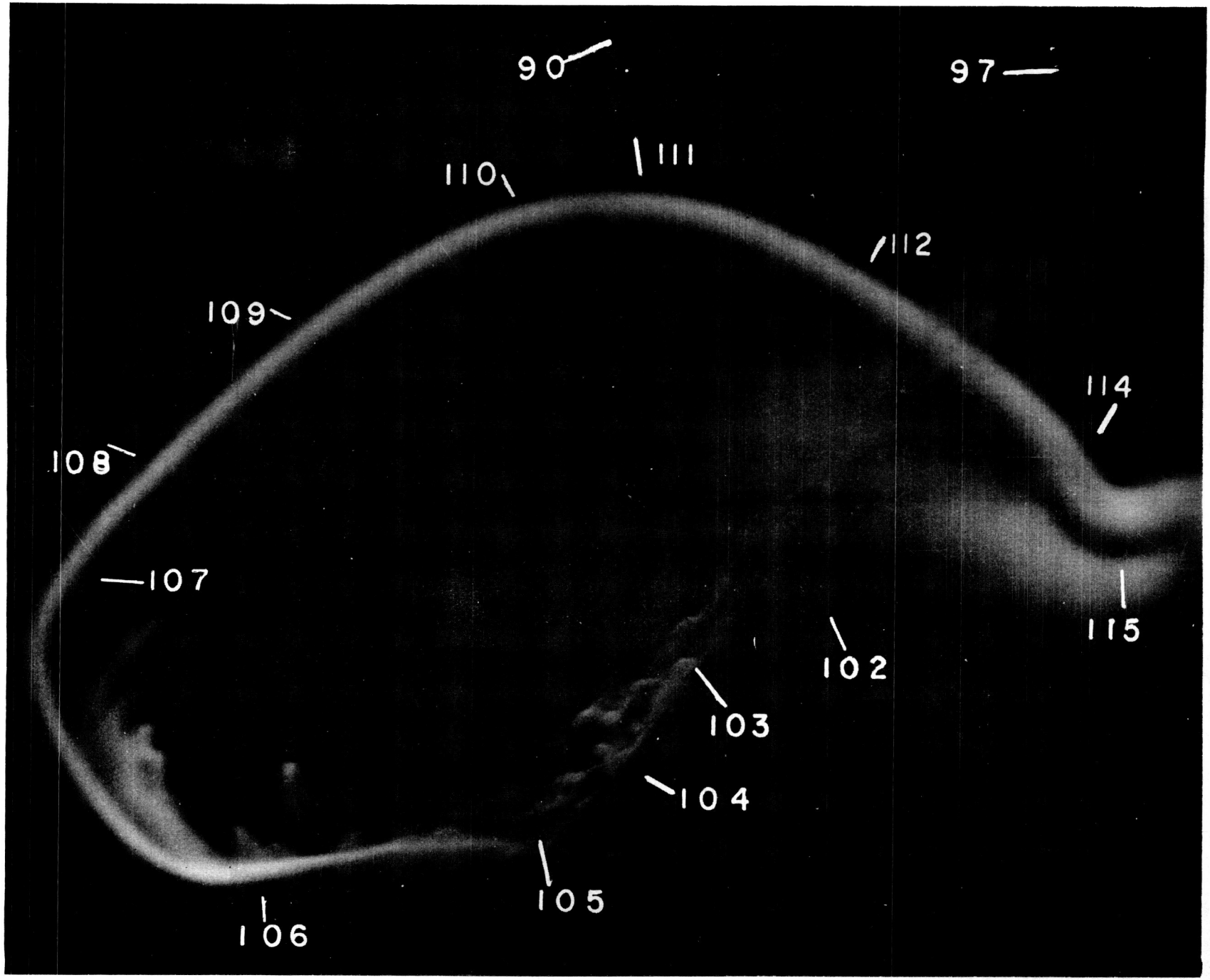

Figure 26. Photograph of vapor trail for 9 December 1960, morning twilight, from Wallops at 480 seconds after launch.

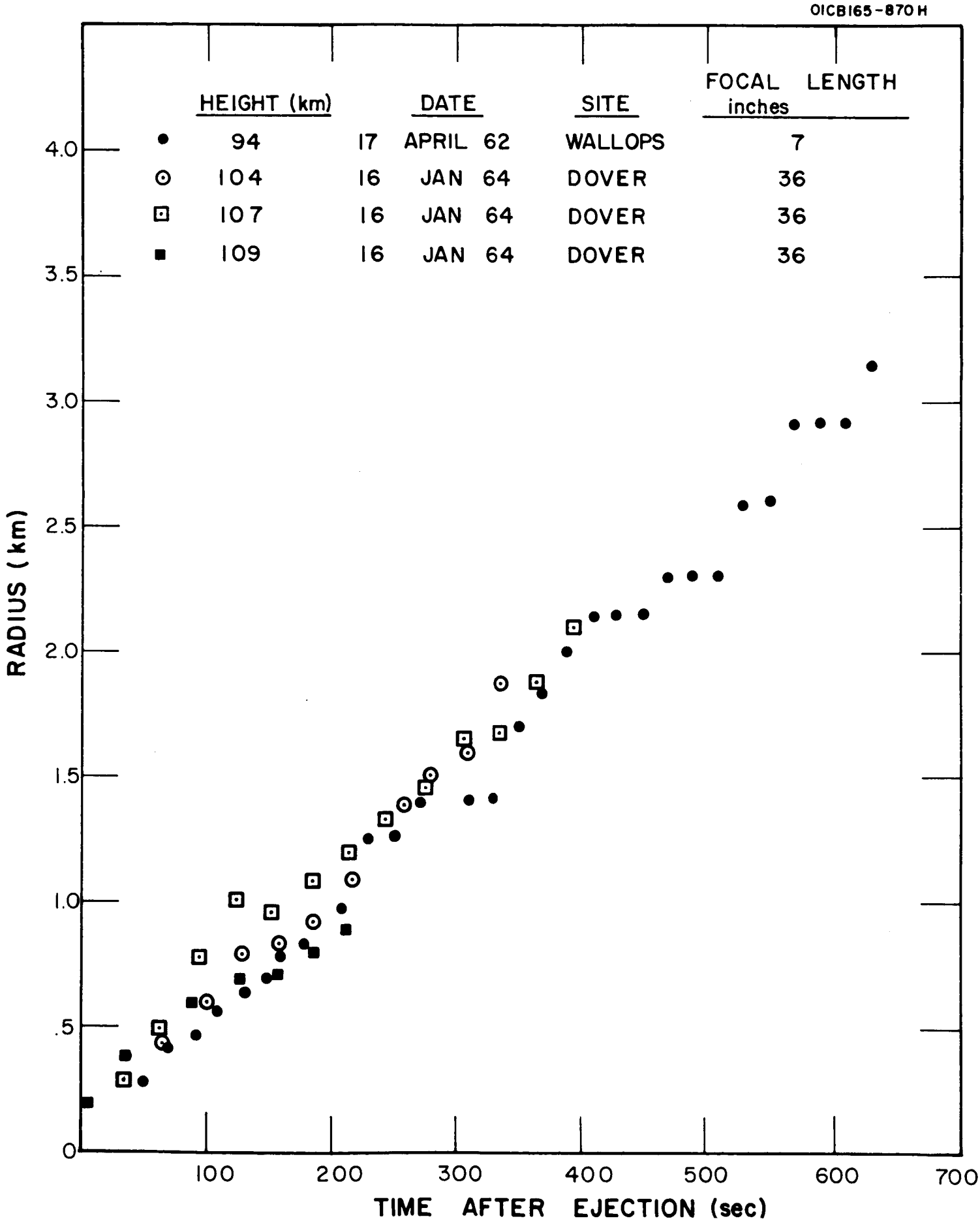

Figure 27. Growth rate of gobule-like structure.

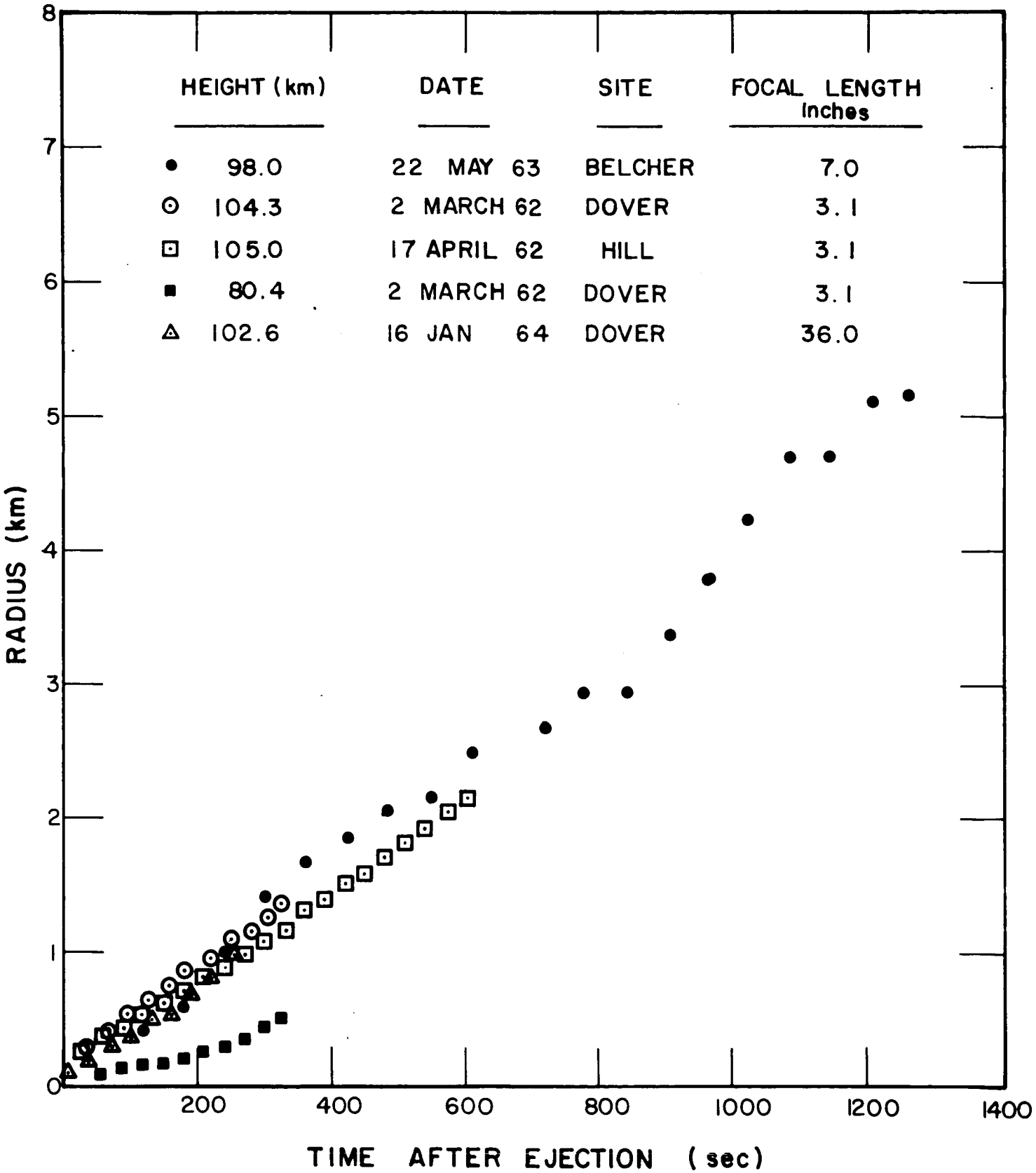

Figure 28. Growth rate of string-like structure.

TABLE 4

TURBULENCE

Date	Height	Growth Rate m/sec	Type	Site
2 March 1962	80.4	1.6		Dover
	85	1.1		
	93.3	2.6		
	95	4.4		
	96	2.2		
	97.6	3.2		
	100.5	5.0		
	101.9	3.6		
	104.3	3.8		
17 April 1962	93	2.7		Hill
	94	4.1	globule	Wallops
	102	4.8		Hill
	105	3.6		Hill
22 May 1963 AM	98.1	4.1		Belcher
	98.1	4.1		Eskimo Point
16 Jan 1964	95	3.4		Dover
AM	102.2	3.55		
	102.6	3.65		
	104	4.7		
	104	5.5	globule	
	107	5.5	globule	
	109	3.35	globule	

difficulties. The rapid growth of the symetrical globules without change of shape is highly uncharacteristic of turbulence as described. The globules have been detected with radius as small as .1 km. Thus the scale of the largest eddies would be about 10 meters. Such small scale eddies would quickly be damped out by the high viscosity at 100 km. The fact that the globules develop in regions of very low shear contradicts the popular theory that the turbulence is produced by the high wind shears that often occur in the same height range. Furthermore, recent theoretical work, suggests that the observed rates of shear at the 100-km level would rarely if ever be able to sustain turbulence.

The observed expansion rates of the globules are not predicted by existing turbulence theory. Although the expansion for early times is theoretically predicted to be linearly proportional to time, a higher power of t dependency should be apparent well within the available times of observations.

The formation and growth of the trail irregularities do not have the characteristics of hydrodynamic turbulence. Thus, one must conclude that the vapor trails do not show evidence that turbulence exists in the atmosphere and that the vapor trail irregularities are due to another phenomenon. Of course, this does not preclude the possibility that the dynamics of the atmosphere are responsible in a manner not yet understood. Another possibility is that the disturbance is in some way connected with the formation of the trail. In fact, there is evidence

in support of such a conclusion. The irregularities occur only when the vapor is being vigorously ejected. This occurs on the upward trail from Wallops Island but not on the down trail since the vaporizer ends rapid burning before reaching the 100-km level on the down part of the trajectory. The down trail is much less dense at 100 km but easily observable and always smooth throughout the region. In some of the French sodium trails in the Sahara, vapor ejection was vigorous at 100 km on both the upward and down trails and the trail becomes irregular in appearance on both trails at the same height. Irregularities in quantity and pressure of the ejected vapor certainly occur but cannot explain the rapid and persistant growth rate.

It has been suggested that exothermic chemical reactions may cause the phenomena.

SECTION 6

CORRELATION OF WIND STRUCTURE AND SPORADIC E

The relationship of wind shear to the formation and existence of Sporadic E has been discussed theoretically by many investigators. Perhaps the most widely accepted hypothesis at the present is due to Whitehead,[11] in which a high horizontal wind shear interacting with the earth's magnetic field will redistribute existing ions into layers with relatively high vertical gradients. An experimental investigation of this relationship was conducted at Wallops Island in November and December of 1962. On three occasions nearly simultaneous measurements of electron density profiles and wind profiles were obtained in the height range 80-130 km. Previous and some more recent experimental comparisons using ground based observations of the ionization profile, have found varying degrees of agreement with the wind shear theory. However, such agreement is not readily apparent in the Wallops data. In fact, close analysis shows some serious disagreement. All of the layers of enhanced ionization do not form in regions of high shear as predicted by the theory. In fact, multiple peaks are apparently independent of the general shear flow. Also the shape of the layers show differences from the prediction,

and the predicted reduction of electron density on either side of a peak is not indicated by the observation. Finally, the sharp layers of enhanced ionization show a striking correlation with small scale wind structure.

A complete discussion of the theory and data has been given by D. Layzer in a paper entitled "Generalization and Critique of the Wind Shear Theory of Sporadic E" and published in the May 1 issue of the Journal of Geophysical Research. Since part of this work was sponsored under this contract, this paper is included as an appendix to this report.

SECTION 7

MEASUREMENTS OF UPPER ATMOSPHERE TEMPERATURE

7.1 THE IMPORTANCE OF TEMPERATURE IN UPPER ATMOSPHERIC PROCESSES

7.1.1 Scale Height. The general law governing a neutral atmosphere is

$$\frac{dp}{p} = \frac{dn}{n} + \frac{dT}{T} = - \frac{dz}{dH}$$

where the scale height is $H = \frac{kT}{mg}$. The behavior of g with height is known from gravitational theory. However the mean molecular weight, m and temperature T cannot be accurately predicted from physical theory and it is obvious that measurements of pressure made at various heights in the atmosphere can only be converted to temperature measurements if assumptions are made about the mean molecular weight. Since oxygen dissociation does not become important below a height of about 100 km, the interpretation of pressure vs height data becomes reasonably simple and unambiguous. However at heights greater than 100 km oxygen dissociation becomes important, and the concentration of the lighter constituents (hydrogen and helium in particular) increases, resulting in a reduction of the mean molecular weight.

Dissociation of molecular oxygen is caused by solar radiation in the Schumann-Runge continuum ($\lambda < 1750\text{Å}$). The recombination coefficient is proportional to $T^{\frac{1}{2}}$ so calculations on the equilibrium of atomic and molecular oxygen will be sensitive to temperature. In addition, the equilibrium mixture will be modified by vertical diffusion, which again is temperature dependent.

7.1.2 Diffusive Separation of Lighter Constituents. In an isothermal atmosphere in diffusive equilibrium, each constituent is distributed with density which varies exponentially with height, ignoring the height dependence of gravity.

That is $n_m \propto \exp(-\frac{z}{H_m}) = \exp(-\frac{z\ m\ g}{kT})$ where H_m is the scale height. This shows that at large heights the concentration of lighter species will be favored, and at the F_2 peak ($z > 300$ km) the atmosphere consists mainly of atomic oxygen and hydrogen. The ratio of these and hence the mean "molecular" weight, cannot be deduced without knowledge of the temperature and temperature gradient. At heights below 100 km mixing, due to winds, turbulence, convection, etc., prevents separation of the constituents. There will also be an increasing amount of argon and helium with increasing height, and again the distribution will be temperature-dependent.

7.1.3 Heat Transfer in the Thermosphere. The thermosphere is a region of increasing temperature as the height rises above 100 km, where the temperature is about 210°K. The temperature and composition changes gradually from that of the earth's atmosphere, to that of the sun's outer

corona, beyond the exosphere. From considerations of the outermost regions of the solar corona Chapman[12] suggests that at the distance of the earth the coronal temperature is in the region 50,000 to 100,000°K. We must therefore have a gradual increase of temperature with height and obviously the higher portions of the earth's atmosphere cannot be considered isothermal. Also the corona becomes a large source of energy for the outer atmosphere, many times greater than the direct radiation received from the sun. The influx of energy cannot be calculated due to lack of accurate data about the distant corona, but it may be derived from knowledge of $\frac{dT}{dz}$ and the thermal conductivity of the atmosphere. Bates[13] however, shows that the heating due to the solar corona will not be conducted down from the exosphere, but will act directly on the thermosphere, the exosphere remaining isothermal. Thus at some height we may expect the temperature increase to become reduced, perhaps at a few thousand degrees K. Bates and McDowell[14] show that to account for the equilibrium between formation and escape of helium the temperature of the exosphere must be about 1900°K.

7.2 MEASUREMENTS OF UPPER ATMOSPHERE TEMPERATURES

The chief source of upper atmosphere temperatures in the region below 100 km has been the grenade experiment. This depends on the fact that the velocity of sound in a gas is equal to $\sqrt{\frac{\gamma RT}{m}}$. Below 100 km γ and m are sufficiently well known to enable the data from grenade explosions to be interpreted as temperatures and winds.

However, above 100 km the grenade method is no longer available due to limitations in the sensitivity of the microphones, and the interpretation depends on the adopted constitution of the atmosphere. Pressure and density data may be obtained to greater heights, and the effect of these on satellite orbits is another source of data at large altitudes. The pressure data cannot yield temperatures without knowledge of m.

Present estimates of temperature in the region above 100 km are based on pressure and density data, certain assumptions having been made about the dissociation of oxygen and nitrogen, and about the diffusive separation of the constituents.

It has been possible to measure upper atmosphere temperatures by observations on the night airglow. However this information is of little use unless the altitude of the emitting layer is also known.

The results of these investigations have been summarized by Armstrong[15] and some of the data are given in Table 5.

These values show the range to be expected. The 1962 Standard Atmosphere would suggest that the last two temperature points correspond more closely to the bottom of the altitude range given.

Following a suggestion by Bates[16] several groups have laid sodium trails in the region 85-220 km, and by means of photographic triangulation have tracked the motions of the trails to give wind data in this region. The light of the trail is due to resonance scattering of

TABLE 5

Emission	Height	Temperature	Observer
OH Rotation Bands	about 70 km	260 $\pm$ 5°K	Meinel, Dufay
OH Rotation Bands	about 70 km	200 $\pm$ 20°K	Gush & Jones
O_2 Atmospheric Bands	about 80 km	150 $\pm$ 20°K	Meinel
Na D lines (twilight)	85 km	240°K	Bricard & Kastler
OI. 5577Å	95 km	155-231°K	Wark & Stone
OI. 5577Å	95 km	180-220°K	Armstrong
OI. 6300Å	116-300 km	< 500°K	Cabannes & Dufay
OI. 5577Å (Aurora)	120-150	330-410°K	Armstrong
OI. 6300Å (Twilight)	150-200 km	750 $\pm$ 150°K	Wark

sunlight. Therefore the Doppler broadened profile of the emission lines should yield information about the temperature of the atoms, since only a few collisions are necessary to reduce the temperature of the trail atoms to the ambient temperature. With sodium trails the situation is not quite so simple. The profile of the line will be modified by the following processes.

(1) The trail may be optically thick resulting in a relative reduction in intensity towards the center of the emission lines. Thus the observed half-width will be greater than the true half-width corresponding to Doppler broadening. The absorption cross-section for the D_2 line (5889.9Å) being twice that of the D_1 line (5895.9Å), the intensity ratio of D_2 to D_1 will be reduced from 2:1 to 1:1 as self-absorption increases. Actually, due to the Fraunhofer D lines in the solar spectrum, the intensity ratio of the illuminating radiation is 0.85 to 1 so the observed intensity ratio for small optical thickness should be 1.7 to 1, decreasing to 0.85 to 1 as the optical thickness becomes much greater than unity.

(2) The illuminating sunlight may have to pass through the terrestrial sodium layer (at about 85 km, extending up to 115 km). This will modify both the profiles and the intensity ratio of the illuminating radiation by an amount which depends on the geometry of the layer and the solar depression.

(3) Hyperfine structure will be apparent at temperatures of about 500°K, or less (17) so analysis would be very difficult even if the composite profile could be observed.

A Fabry-Perot interferometer has been used in observations on a sodium vapor trail.[18] Even where the trail was faint, and therefore optically least dense, it was shown that the D_2/D_1 ratio of sodium did not increase above 1.4, and the profiles obtained were considerably broader than could be attributed to any reasonable temperature at the trail height ($h \leq 215$ km). It is interesting to note that the twilight resonance radiation of the natural sodium layer, when it is least intense, never reaches a D_2/D_1 ratio of 1.7.[19,20]

Following the observation of the second resonance doublet of sodium in vapor trail releases[21,22,23] it was thought that perhaps other emission lines of sodium should be present, which would not suffer from self-absorption. Any line will suffer self-absorption if its lower level is the ground state of the atom. In addition the profile of an emission line may be modified if its upper level is populated by a transition which is subject to self-absorption. An examination of all the spectra of the alkali metals was made and it was concluded that the 8126Å doublet of lithium would be most suitable for temperature determinations[24] for the following reasons:

(1) It complies with both the conditions stated above so that the line profile should not be modified by self-absorption.

(2) There is no strong twilight or night airglow emission near to 8126Å.

(3) There is no strong atmospheric absorption near 8126Å.

(4) The hyperfine structure splittings are so small as to cause no measurable distortion of the profiles above 200°K.

The intensity of the sodium emission is about 1 photon/sec atom. However as the trail is optically thick it is expected that the effective emission rate is considerably less than this. The calculated emission rate for the lithium doublet in the same circumstances is about 10^{-2} photon/sec atom. Since the trails are optically thick, the intensity seen is limited by the available energy in the solar spectrum. In the case of the lithium 8126Å lines, the energy is limited by the available solar energy at 3232Å. Due to the two isotopes of lithium, the lines appear to be a triplet, the isotope splitting being almost equal to the fine structure splitting.

Therefore an attempt was made to observe the intensity of the 8126Å doublet from a trail of lithium and sodium vapor laid be Nike-Apache rockets launched from Wallops Island. Several photometers using birefringent filters of the type described by Dunn and Manring[25] were available. As these incorporated half- and quarter-wave retarding plates, which only behave as such near 5500Å, it was felt that the depth of modulation achieved at 3232Å and 8126Å would be very small. Thus the filter wheels were modified to enable the dielectric filters to be rocked. This enabled the photometer to scan from λ_{max} to λ_{min} and back again. The wavelength sweep was made approximately a linear function of time, by cutting the cam suitably. It was found that during a scan, which lasted about three seconds, the peak transmission of the filter diminished, and the bandwidth increased, in such a manner that a continuum produced little modulation of the output current, but that a line source caused sharp peaks to appear on the recording. A phase

marker was also recorded so that the position of the peak could be determined, and it was also found that a wavelength could be identified by the waveform it produced. The output from the photomultiplier was passed through a DC amplifier and recorded.

The four rockets in the January 1964 series were launched as follows:

Two at evening twilight. Due to rocket malfunction, neither of these trails reached sufficient altitude to be useful for these observations.

One about midnight. The trail appeared briefly as sodium D line emission. No emission at 8126Å was seen, or expected.

One at morning twilight. Contrary to expectation, no 8126Å radiation was seen.

The filters on the photometer were chosen to examine the brightness of the sodium D lines, the first resonance lines of lithium, the 0-0 band of aluminum oxide, and the 8126Å lines of lithium. The analysis of the records to give an intensity-time plot is not yet complete, but the 8126Å radiation, if any, was undetectable.

The appearance of the 3303Å doublet of sodium is somewhat sporadic, both in frequency and intensity. It has only been seen at morning twilight, and the intensity ratio 5893Å/3303Å has values ranging from 1 to 100. It is difficult to explain this phenomena. The ozone absorption, peaking at 2650Å, is fairly low in the region 3200Å-3300Å, and

the density of ozone above 50 km is not great. Further investigation of this topic is required. It is possible that photochemical action is responsible for the higher intensities of 3303Å radiation.

7.3 TEMPERATURE MEASUREMENTS USING THE 6707Å DOUBLET OF LITHIUM

Some of the disadvantages of using sodium trails may be overcome by using lithium. There is no Fraunhofer line at these wavelengths, the earth's atmosphere contains practically no lithium, and there is no twilight enhanced layer against which the lithium radiation must be measured. We still require to deal with self-absorption, fine structure, hyperfine structure, and isotope splitting. A means of dealing with all but the foremost exists.

The profile of a spectral line of zero width, when seen through a Fabry-Perot interferometer, is given by the Airy function

$$I(x) = \frac{\frac{T^2}{(1-\rho)^2}}{1+\frac{4\rho}{(1-\rho)^2}\,\mathrm{Sin}^2\,\pi x}$$

where T and ρ are the transmission and reflection powers respectively of the reflecting layers, and x is given by

$$x = \frac{2\tau\,\mathrm{Cos}\,\phi}{\lambda}$$

where τ is the interferometer plate spacing, λ is the wavelength and ϕ is the angle between the direction of view and the normal to the plates.

Krebs and Sauer[26] have shown that this may also be expressed as a Fourier series, which, neglecting a constant multiplier is

$$I(x) = 1 + 2 \sum_{n=1}^{\infty} \rho^n \text{ Cos } 2\pi \text{ nx} .$$

Each term in the expansion may now be convolved with the Gaussian distribution function corresponding to a Doppler broadened line, yielding

$$I(x) = 1 + 2 \sum_{n=1}^{\infty} \rho^n \exp(-A' \mu^2 n^2) \text{ Cos } 2\pi \text{ nx}$$

where A' is a constant, and μ is the Doppler width of the line expressed in terms of the spectral range of the interferometer.

It has been shown[27] that if a scanning Fabry-Perot is made to oscillate so that the optical thickness follows a saw-tooth waveform as a function of time, and if the amplitude of oscillation is an integral number of half-wavelengths, the output from a photomultiplier observing an infinitesimally small region at the center of the fringe system will be given by

$$i(t) = 1 + 2 \sum_{n=1}^{\infty} \rho^n \exp(-A' \mu^2 n^2) \text{ Cos } 2\pi \text{ n } \omega t.$$

Where there are M wavelength components in the fine, and hyperfine structure of the line, and where the scanning hole has a finite radius ρ' (orders), the output will now be given by

$$i(t) = 1 + 2 \sum_{m=1}^{M} \sum_{n=1}^{\infty} I_m \rho^n \frac{\text{Sin } \theta_{n,m}}{\theta_{n,m}} k_n \exp(-A' \mu^2 n^2) \text{ Cos}(2\pi n \omega t - \Delta)$$

where

$$k_n = \sqrt{\left(\sum_m I_m \text{ Cos } 2\pi n \delta_m''\right)^2 + \left(\sum_m I_m \text{ Sin } 2\pi n \delta_m''\right)^2}$$

and

$$\theta_{n,m} = \pi n \rho_m' = \frac{\pi n \tau r^2}{\lambda_m f^2}$$

where I_m and λ_m are the intensity and wavelength of the m^{th} component,

r is the physical radius of the scanning hole

δ_m'' is $\frac{2\tau(\lambda_m - \lambda_1)}{\lambda^2}$

In the case of lithium the components arise in different isotopes. This may be allowed for by writing I_m' for I_m in the above expression, and putting

$$I_m' = I_m \exp[-A' n^2(\mu_p^2 - \mu_o^2)]$$

$$= I_m \exp[-7.307433 \times 10^{-12} \frac{\tau^2 n^2 T}{\lambda^2} (\frac{1}{m_p} - \frac{1}{m_o})]$$

where m_p is the mass of the predominant isotope

m_o is the mass of the other isotope

We now use m_p in deriving temperature (T) from the amplitudes of the harmonics. It may also be shown that the effect of plate dishing, or of plate irregularity distributed according to a known distribution function may be allowed for.

Reverting to the simple case where we have only one emission line, we have

$$A_n = \rho^n \exp(-A' \mu^2 n^2)$$

where A_n is the amplitude of the n^{th} harmonic in the signal output. It may easily be shown that by considering the first three harmonics

$$A' \mu^2 = \text{Log} \frac{A_2}{\sqrt{A_1 A_3}}$$

and since

$$\mu^2 = \frac{Q T \tau^2}{m \lambda^2} ,$$

where Q is a constant, we have

$$T = Q' \frac{m \lambda^2}{\tau^2} \quad \text{Log} \frac{A_2}{\sqrt{A_1 A_3}}$$

where Q′ is another constant.

Thus, by extracting the amplitudes of the first three harmonics from the signal and performing some arithmetic by simple analog circuits, the temperature may be indicated directly.

Where self-absorption is present, the distribution of energy with wavelength will no longer follow a Gaussian profile. Thus, if we take the first four harmonics, and solve in four different ways for T we will get four different temperatures. The convergence of these will indicate a diminishing self-absorption effect and a closer approach to the true

temperature. It might even be possible to derive a relationship between the indicated temperatures and the true temperatures, when self-absorption is apparent. An analytical approach to this has been attempted, with some success, but there is no certainty that the distribution function assumed[28] will accurately represent the true case.

Accuracy of the method. Obviously the larger we make the scanning hole, the larger the signal becomes. However, the depth of modulation decreases according to $\frac{\text{Sin } \theta_{m,n}}{\theta_{m,n}}$ and there will be an optimum choice to suit the combination of the three harmonics. In addition, enlarging the scanning hole allows more of the background continuum to be detected, and increases the area of the detector with a consequent increase in dark current.

It may be shown that the signal-to-noise ratio of the n^{th} harmonic is given by S_n, where

$$S_n^2 = \frac{\epsilon\left(\frac{\sigma-1}{\sigma}\right) BAT_L T_F S \frac{T_D^2}{(1-\rho)^2} \rho^n \sqrt{2}\, \pi \frac{r^2}{f^2} \frac{\text{Sin } \theta_n}{\theta_n} \frac{\exp\left(-\frac{\eta\tau^2 Tn^2}{m_A \lambda^2} k_n\right)}{1+2Q}}{3{\cdot}2 \times 10^{-19}\left(\left\{BAT_L T_F S \frac{T_D^2}{(1-\rho)^2} \pi \frac{r^2}{f^2} \frac{1}{1+2Q}\right\} + \pi r^2 DS + \frac{SCAT_L T_F r^2 W(1-\rho)}{f^2 \sqrt{\rho}}\right)\Delta f}$$

where $$Q = \sum_{n=1}^{\infty}\left[\rho^n \exp\left(-\frac{\eta\tau^2 Tn^2}{m_A \lambda^2}\right)\frac{\text{Sin } \theta_n}{\theta_n} k_n\right]$$

$$\theta_n = \frac{\pi n \tau r^2}{\lambda f^2}$$

B = trail brightness, photons/cm^2 sec sterad

A = area of Fabry-Perot plates

T_L = transmission of lenses, etc.

T_F = transmission of narrow band filter at 6707Å

S = sensitivity of photo cathode, amps/photon sec^{-1}

D = equivalent photon dark current cm^{-2}

C = continuum sky brightness photons/cm^2 sec sterad Å

W = width at half transmission of filter

Δf = bandwidth of electronic filters isolating harmonics

σ = gain/stage of the photomultiplier

ϵ = fraction of photo cathode electrons collected by the first dynode

Since each harmonic has a mean value and an rms fluctuation about the mean, we expect a mean temperature T' and an rms fluctuation ($\Delta T'$) about this mean.

We find

$$T' = 3{\cdot}151011 \times 10^{11} \frac{m_A \lambda^2}{\tau^2} \left\{ \left[L_2 - \frac{1}{2}(L_1 + L_3) \right] + \left[\text{Log}_{10} \sqrt[4]{\frac{\left(1+\frac{1}{S_1^2}\right)\left(1+\frac{1}{S_3^2}\right)}{\left(1+\frac{1}{S_2^2}\right)^2}} \right] \right\}$$

where $L_n = \text{Log}_{10} A_n$

and

$$\Delta T' = 0{\cdot}9018197 \times 10^{11} \frac{m_A \lambda^2}{\tau^2} \left\{ \sqrt{\text{Log}_{10}\left(1+\frac{1}{S_2^2}\right)} + \frac{1}{2}\left(\sqrt{\text{Log}_{10}\left(1+\frac{1}{S_1^2}\right)} + \sqrt{\text{Log}\left(1+\frac{1}{S_3^2}\right)} \right) \right\}$$

The foregoing relationships have been programmed for the IBM 1620 computer, and it has been shown that the error due to $\Delta T'$ is always much larger than that due to T', by a factor of perhaps 10^3. From these computations the optimum values of τ and r may be chosen.

In favorable circumstances, taking 2 minutes for a measurement, the error may be as low as $10^{\circ}K$. Because of the logarithms in the equation, it has been found that $\Delta T'$ is independent of temperature to a first approximation. Hence the percentage accuracy increases with temperature.

One important feature of this method is that it is independent of actual knowledge of the reflectivity ρ. In previous determinations of temperature from Fabry-Perot interferograms it has been necessary to compute a series of profiles for various temperatures and to obtain the indicated temperature by interpolation. To compute the profiles, the reflectivity must be known. It is a familiar source of error that the reflectivity is measured at a different time, and usually at a lower order, to that used in the actual experiment. In this case slight changes in reflectivity, due to deterioration of the coatings, will not influence the process. However, large changes will reduce the depth of modulation and the inaccuracy, expressed as $\Delta T'$ will increase, although T' will not change.

SECTION 8

CONCLUSIONS AND RECOMMENDATIONS

8.1 WIND STRUCTURE

The experimentally determined wind model suggests a new picture of the wind structure in the 80 to 135 km height region. On the basis of the model, the entire wind vector in the region may be represented by a relatively small prevailing component and three quasi-periodic harmonics. Thus the major part of the resultant wind may be attributed to thermal or tidal driving forces. The model is based on limited data but does fit the data and shows some ability to predict, since several points were added after the model figures were drawn. No serious physical objections have so far been raised.

The most obvious experimental approach for verification of the model is a continuous observation of the winds over one or more complete cycles. Since no method of measuring winds over the entire altitude range during the daytime is available, this cannot be done at present. However, this restriction may not be too serious. First, continuous observations are not required. Measurements every two or three hours should be sufficient. Second, methods are available for nighttime measurements and these, together

with twilight observations could cover more than a half cycle at some seasons. Several such series are recommended to verify the Wallops model. Complete understanding of the wind structure will require observations during the day. Thus, it is also recommended that methods be developed for measurement of winds during the daytime. Complete understanding of the wind structure also requires observations from other latitudes. Of particular interest are the equatorial and polar regions.

8.2 DIFFUSION AND TEMPERATURE

The measured diffusion coefficients show variations from those computed with the most recent Standard Atmospheres. However, the comparison requires both temperature and number density. An independent measurement of temperature along with the diffusion measurement would allow determination of the number density. For this reason, development of a method of temperature determination is recommended. Refinement of the methods, together with diffusion measurements for other atoms with varying molecular weights may also allow determination of the mean molecular weight of the ambient.

8.3 TURBULENCE

Detailed analysis of the formation and growth of the irregular region of vapor trails around 100 km shows that the trails do not have the characteristics that are expected if the cause were hydrodynamic turbulence in the ambient atmosphere. Thus, some other source of the irregularities must be found. The long focal length camera, acquired for this purpose,

produced very useful observations of the only available trail on which it was used. It is recommended that more such cameras be obtained in order to completely investigate this phenomenon.

8.4 CORRELATION OF WINDS WITH SPORADIC E

The data obtained from three nearly simultaneous measurements of winds and electron-density profiles, have suggested new theories concerning the relation of winds and sporadic E. More such measurements are urgently needed to study this relationship. Simultaneous measurements of the Earth's magnetic field would add greatly to the information.

8.5 THEORETICAL STUDY

The results to date suggest a number of significant theoretical problems. These fall into two groups: studies of the nonlinear, periodic oscillations of the upper atmosphere; and studies of the fine structure of the wind system and its connection with sporadic E. It is highly desirable that these theoretical studies be carried on in close contact with the experimental work, since the two activities are mutually stimulating.

The number of problems relating to nonlinear oscillations that have been thoroughly investigated up to now is small. Some examples of forced, nonlinear oscillations have been studied, and these throw a little light on the problem at hand. For example, they enable one to understand, in a general way, how the 8-hour oscillation could be dominant in the response of the atmosphere even though it is weak or even absent in the driving force. The atmosphere differs from the systems that have been studied

to date in nonlinear mechanics, in that it is a system in which energy propagates. Energy is fed into the system near the surface of the Earth, propagates upward, and finally escapes or is dissipated above 135 km. Layzer has suggested that the upper boundary condition plays an essential role in this phenomenon. Since the top of the atmosphere is much more susceptible to the variable part of the solar radiation than the bottom, it may indeed, be the seat of the observed phase variability. Perhaps the best way to attack the problem quantitatively would be to devise simplified models incorporating the essential properties of energy propagation and a variable upper boundary condition.

The hydromagnetic interpretation of the fine structure of the wind profiles suggested by Layzer can be formulated mathematically. This leads to a pair of coupled partial differential equations whose solutions describe the way in which the velocity field (wind profiles) and the magnetic field develop in time. Approximate solutions to these equations would make possible a quantitative check of the theory.

REFERENCES

1. Manring, E., Bedinger, J., Knaflich, H., and Lynch, R., "Upper Atmospheric Wind Profiles Determined from Three Rocket Experiments," GCA Technical Report 61-1-N (February 1961).

2. Manring, E. and Knaflich, H., "Some Measurements of the Coefficient of Diffusion in the Upper Atmosphere," GCA Technical Report 61-3-N (March 1961).

3. National Aeronautics and Space Administration, Contract NAS5-215, Final Report, "Study of Winds, Diffusion and Expansion of Gases in the Upper Atmosphere," GCA Technical Report No. 62-13-N (October 1962).

4. National Aeronautics and Space Administration, Contract NASw-396, Final Report, "Study of Winds, Diffusion, and Expansion of Gases in the Upper Atmosphere," GCA Technical Report No. 63-16-N (May 1963).

5. Rosenberg, N. W., Golomb, D., and Allen, Jr., E. F., "Chemiluminescence of Trimethyl Aluminum Released into the Upper Atmosphere," J. Geophys. Res., 68, 5895-5898 (1963).

6. Rosenberg, N. W., Golomb, D., and Allen, Jr., E. F., "Chemiluminescent Techniques for Studying Nighttime Winds in the Upper Atmosphere," J. Geophys. Res., 68, 3328-3330 (1963).

7. Edwards, H. D., Justus, C. G., and Kurts, D. C., "Evening Twilight Winds from 68 to 140 Kilometers for May 21, 1963," J. Geophys. Res., 68, 6062-6063 (1963).

8. Manring, E., Bedinger, J., Knaflich, H., and Layzer, D., "An Experimentally Determined Model for the Periodic Character of Winds from 85 to 135 km," GCA Technical Report No. 63-27-N (November 1963).

9. Manring, E., Bedinger, J., and Knaflich, H., "Some Measurements of Winds and of the Coefficient of Diffusion in the Upper Atmosphere," Space Research II, Proceedings of the Second International Space Science Symposium Florence, April 10-14, 1961, p. 1107-1124, edited by H. C. van de Hulst, C. de Jager, and A. F. Moore, North-Holland Publishing Co., Amsterdam (1961).

10. Coté, Owen, "On the Question of Turbulence in the Upper Atmosphere," GCA Technical Report No. 62-12-N (October 1962).

11. Whitehead, J. D., "The Formation of a Sporadic-E Layer from a Vertical Gradient in Horizontal Wind," in Ionospheric Sporadic E, edited by E. K. Smith, Vol. 2, pp. 276-291, Pergamon Press, Oxford (1962).

12. Chapman, S., The Threshold of Space (ed. M. Zelikoff) p. 65, Pergamon Press, London (1957).

13. Bates, D. R., Proc. Roy. Soc., A, 253, 451 (1959).

14. Bates, D. R., and McDowell, M. R. C., J. Atmospheric and Terrest. Phys., 11, 200 (1957).

15. Armstrong, E. B., J. Atmospheric and Terrest. Phys., 13, 205 (1959).

16. Bates, D. R., J. Geophys. Res., 55, 347 (1950).

17. Chamberlain, J. W., Hunten, D. M., and Mack, J. E., J. Atmospheric and Terrest. Phys., 12, 153 (1958).

18. Armstrong, E. B., and Best, G. T. (to be published).

19. Harrison, A. W., and Jones, A. V., The Airglow and Aurorae (Ed. Armstrong, E. B., and Dalgarno, A.) 95 (1956).

20. Jones, A. V., and McPherson, D. H., J. Atmospheric and Terrest. Phys., 12, 166 (1958).

21. Cooper, C. D., Manring, E. R., and Bedinger, J. F., J. Geophys. Res., 63, 369 (1958).

22. Vassy, A., and Vassy, E., C. R. Acad. Sci. Paris, 248, 2235 (1959).

23. Vassy, A., and Vassy, E., Planet. Spa. Sci., 2, 71 (1959).

24. Best, G. T., and Patterson, T. N. L., Planet. Spa. Sci., 9, 521 (1962).

25. Dunn, R. B. and Manring, E. R., J.O.S.A., 46, 572 (1956).

26. Krebs, K., and Sauer, A., Ann. der Physik., 6, 359 (1953).

27. Best, G. T. (to be published).

28. Mitchell, A. C. G., and Zemansky, M. W., "Resonance Radiation and Excited Atoms," 109 (1934).

APPENDIX A

GENERALIZATION AND CRITIQUE OF THE WIND-SHEAR THEORY OF SPORADIC E*

David Layzer

Harvard College Observatory, Cambridge, Massachusetts

*Journal of Geophysical Research 69, 1853-1860 (1964).

ABSTRACT

Previous discussions of the hypothesis that sporadi E layers result from a redistribution of existing ionization caused by vertical ionization drift have rested on special and somewhat unrealistic assumptions. This paper formulates the hypothesis in a more general way and compares its implications with recent experimental results concerning the structure of E_s layers and the connection between ionization profiles and wind profiles in the E region. The main results of the paper are as follows: (1) The predicted ionization profiles have cusp-like peaks (rounded off by diffusion) of variable width, the width of a peak being inversely proportional to the square of its height. Theory also predicts a substantial reduction of the electron density on either side of a peak. By contrast, observed ionization profiles have nearly rectangular peaks of uniform width ($\lesssim$ 1 km) and variable height ($1 \leq N_{max}/N_o \lesssim 10^2$) superimposed on an apparently unperturbed background. (2) Theoretically, layers of enhanced ionization will form in regions where the wind shear is exceptionally high. Observation shows that the reverse is true. (3) The fractional changes that can be produced by vertical ionization drift appear to be considerably smaller than those observed to be associated with E_s layers.

A related hypothesis, that layers of enhanced ionization form through the trapping of vertically drifting ionization by narrow turbulent layers, also conflicts with experiment.

A.1 INTRODUCTION

There now exists a sufficiently detailed body of experimental information about electron densities[A-1,A-2] and horizontal winds[A-3] in the lower E region to afford a decisive test of the hypothesis that E_s layers result from a redistribution of existing ionization caused by vertical ionization drift. Whitehead[A-4,A-5] and Axford[A-6] have worked out the consequences of this hypothesis in some detail, but under rather special assumptions. Both authors represented the wind profile (the horizontal wind as a function of height) by a plane sine curve and both postulated that horizontal polarization fields are absent. Neither of these assumptions is realistic. In addition, some of the conclusions of Axford and Whitehead concerning ionization profiles produced by the drift mechanism depend on the results of numerical integrations. These circumstances make it difficult to separate the essential features of the wind-shear theory from those that depend on special assumptions and particular choices of parameters. The purpose of the present paper is accordingly twofold: to cast the wind-shear theory in a form that is sufficiently general to permit comparison with experiment and yet sufficiently simple to permit approximate solutions of the fundamental equations to be obtained in closed form; and to decide whether the theory is consistent with existing experimental information about sporadic E.

For the sake of simplicity, we limit our considerations at the outset to middle latitudes and to a small height range centered on 100 km. We also make the usual "slab" approximation; that is, we assume that a vertical polarization field inhibits vertical electric currents. The horizontal components of the current density are then related to the horizontal components of the electric field by the equation

$$\begin{pmatrix} j_x \\ j_y \end{pmatrix} = \begin{pmatrix} \sigma_{xx} & \sigma_{xy} \\ \sigma_{yx} & \sigma_{yy} \end{pmatrix} \begin{pmatrix} E_x \\ E_y \end{pmatrix} \tag{A-1}$$

where (under our assumptions) the components of the conductivity tensor are given by

$$\sigma_{xx} = \sigma_1 \operatorname{cosec}^2 \chi, \quad \sigma_{yy} = \sigma_1, \quad \sigma_{xy} = -\sigma_{yx} = \sigma_2 \operatorname{cosec} \chi \tag{A-2}$$

$$\sigma_1 = \frac{Ne}{B} \frac{\omega_i}{\nu_i}, \quad \sigma_2 = \frac{Ne}{B} \tag{A-3}$$

The x-axis points north, the y-axis west; χ denotes the magnetic dip angle, N the electron density, B the magnitude of the magnetic field, ω_i the gyrofrequency of the ions, and ν_i the collision frequency of the ions. In the height range under consideration

$$\frac{\omega_i}{\nu_i} \approx \frac{1}{10} \tag{A-4}$$

and this fact, along with the assumption that $\sin\chi \approx 1$, has been used to simplify the above formulas.

A.2 THE RELATION BETWEEN DRIFT SPEED AND WIND VELOCITY

In the presence of a magnetic field, an applied electric field will cause the electrons and ions to drift in directions that are not in general strictly anti-parallel, so that in some direction the electrons and ions will have a common velocity component, representing a drift of neutral ionization. On the assumption that the number densities of electrons and ions are equal, the current density is given, in an obvious notation, by

$$\underset{\sim}{j} = - Ne(\underset{\sim}{V}_e - \underset{\sim}{V}_i) \equiv - Ne\underset{\sim}{v} \qquad (A\text{-}5)$$

The drift velocity of neutral ionization is perpendicular to the current density and is given by

$$\underset{\sim}{V}_d = \frac{\underset{\sim}{v} \times (\underset{\sim}{V}_i \times \underset{\sim}{V}_e)}{v^2} \qquad (A\text{-}6)$$

In the circumstances under consideration, Martyn[A-7] has shown that the vertical component of $\underset{\sim}{V}_d$ is given by

$$w = - \frac{\omega_i}{\nu_i} \frac{j_y}{Ne} \cos\chi \qquad (A\text{-}7)$$

Thus the vertical drift speed is proportional to the eastward component of the electric current and to the horizontal component of the magnetic field.

Equation (A-1) relates the current density to the electric field, which is made up of two physically distinct parts:

$$\underset{\sim}{E} = \underset{\sim}{E}^{dyn} + \underset{\sim}{E}^{pol} \tag{A-8}$$

The dynamo field is given (in e.m.u.) by

$$\underset{\sim}{E}^{dyn} = \underset{\sim}{V} \times \underset{\sim}{B} = B \sin\chi \, (-V_y \, \underset{\sim}{\hat{x}} + V_x \, \underset{\sim}{\hat{y}}) \tag{A-9}$$

where $\underset{\sim}{V}$ denotes the horizontal wind. The polarization field results from the flow of horizontal currents. Once the velocity field (wind system) has been specified, the condition that the current system must be closed serves to determine the polarization field.[A-8] In certain circumstances, the steady-state polarization field completely inhibits the flow of Hall current. The apparent direct conductivity in the y-direction (i.e., the ratio j_y/E_y^{dyn}) is then increased from σ_{yy} to

$$\sigma_{yy} + \frac{\sigma_{xy}^2}{\sigma_{xx}} = \sigma_1 + \frac{\sigma_2^2}{\sigma_1} \approx \frac{Ne}{B} \frac{\nu_i}{\omega_i} \tag{A-10}$$

The westward component of the current density and the vertical drift speed of neutral ionization corresponding to (A-10) are

$$j_y = + Ne \frac{\nu_i}{\omega_i} \sin\chi \, V_x, \quad w = - \frac{1}{2} V_x \sin 2\chi \tag{A-11}$$

The drift speed is proportional to the southward component of the neutral wind and goes to zero at the magnetic equator as well as at the magnetic poles.

Whitehead and Axford assumed, in effect, that polarization fields do not build up. Instead of (A-11) one then obtains

$$j_y = NeV_y, \quad w = -\frac{\omega_i}{\nu_i} V_y \cos\chi \tag{A-12}$$

The vertical drift speed is proportional to the eastward component of the neutral wind and increases with decreasing geomagnetic latitude.

In general we may write

$$w = a_x V_x + a_y V_y = \underset{\sim}{a} \cdot \underset{\sim}{V} \tag{A-13}$$

leaving the constant vector $\underset{\sim}{a}$ unspecified. To evaluate $\underset{\sim}{a}$, one would need to carry out a calculation similar to Baker's[A-8] calculation of the electric fields and currents resulting from tidal motions in the upper atmosphere.

A.3 THE ELECTRON-DENSITY PROFILE

If we assume that the neutral wind is horizontal and depends only on the vertical coordinate z, the equation of continuity for the electron (or ion) density N takes the form

$$\frac{\partial N}{\partial t} + \frac{\partial (Nw)}{\partial z} = q - \alpha N^2 + D \frac{\partial^2 N}{\partial z^2} + \frac{g}{\nu_i} \frac{\partial N}{\partial z} \tag{A-14}$$

where q is the rate of ionization, α the recombination coefficient, D the ambipolar diffusion coefficient, and g the acceleration of gravity. We may ignore variations of q, α, and D over the height and time intervals of interest here. We may also neglect the gravitational drift speed g/ν_i ($\approx$ 2 cm/sec) in comparison with w. Finally, we assume that the characteristic time associated with changes of the velocity field is

long compared with the characteristic time for redistribution of ionization by vertical drift. If τ is a characteristic period of the velocity field, this assumption requires $\tau/2\pi \gg |dz/dw|$ which will be satisfied if τ is of the order of several hours. We may then drop the first term on the left side of (A-14) and neglect the time dependence of N and w. Equation (A-14) reduces, finally, to the ordinary, nonlinear differential equation

$$\frac{d}{dz}(Nw) = q - \alpha N^2 + D\frac{d^2N}{dz^2} \qquad \text{(A-15)}$$

The remainder of this section treats the still simpler equation

$$\frac{d}{dz}(Nw) = q - \alpha N^2 \qquad \text{(A-16)}$$

which describes the redistribution of ionization by vertical ionization drift in the absence of diffusion. The next section considers the effects of diffusion.

If the electron-density profile N(z) has a peak at some level $z = z_o$, the product w(dN/dz) must vanish there and (A-16) reduces to an algebraic equation whose solution is

$$N(z_o) = N_1 \equiv N_o[(1 + \tfrac{1}{4}\eta^2)^{\frac{1}{2}} + \tfrac{1}{2}\eta] \qquad \text{(A-17)}$$

where N_o, the equilibrium value of N is given by

$$N_o = \left(\frac{q}{\alpha}\right)^{\frac{1}{2}} \qquad \text{(A-18)}$$

and the pure number η is given by

$$\eta = - \frac{w_o'}{\alpha N_o} , \quad w_o' \equiv \left. \frac{dw}{dz} \right|_{z=z_o} \tag{A-19}$$

From (A-17) and (A-19) it is clear that if $N_1 \gg N_o$, then w_o', the gradient of the vertical drift velocity, must be large and negative. We may accordingly approximate w(z) in the neighborhood of an electron-density peak by the first two terms in its Taylor expansion:

$$w(z) = w_o + w_o'(z - z_o) \tag{A-20}$$

We can now solve Equation (A-16) exactly. We first change the independent variable from z to w, to obtain

$$w_o' \frac{d\psi}{dw} + \alpha w^{-2} \psi^2 - q = 0, \quad \psi \equiv wN \tag{A-21}$$

The further transformations

$$w = \frac{1}{u} , \quad \psi = - \frac{w_o'}{\alpha} \frac{1}{v} \frac{dv}{du} \tag{A-22}$$

yield the linear, second-order, differential equation

$$u^2 \frac{d^2 v}{du^2} - k(k - 1) v = 0 \tag{A-23}$$

where

$$k(k - 1) = \eta^{-2} \tag{A-24}$$

The general solution of (A-23) is

$$v = Au^{k_1} + Bu^{k_2} \tag{A-25}$$

where k_1, k_2 are the roots of the quadratic Equation (A-24) given by

$$k_1, k_2 = \tfrac{1}{2}[1 \pm \sqrt{(1 - 4\eta^{-2})}] \tag{A-26}$$

Finally, N(z) is given by

$$N(z) = -\frac{w_o'}{\alpha} \frac{k_1 + k_2 C w^{k_1 - k_2}}{1 + C w^{k_1 - k_2}} \tag{A-27}$$

For negative values of w the constant C must be chosen so as to make $C w^{k_1 - k_2}$ real.

Since $k_1 > 1$ and $k_2 < 0$, it follows from (A-27) that, for any given value of C, N(z) either increases or decreases monotonically with w. Thus dN/dz never vanishes, except in the trivial case C = 0, for which N = const. Since w(dN/dz) = 0 at an electron-density peak, it follows that w itself must vanish there. Conversely, if $w_o = 0$ and $w_o' < 0$, Equation (A-14) shows that the electron-density profile will develop a peak at the level $z = z_o$. We have thus proved that the electron-density profile has a peak at a given level if and only if the drift speed vanishes and its gradient is negative there. This conclusion needs to be modified only slightly to allow for diffusion, which causes little change in the position of a peak.

At a level where the drift speed vanishes, the electron-density gradient may be discontinuous. Hence, the value of the constant C in (A-27) need not and in general will not be the same above and below such a level. Symbolically, we have, with the help of (A-17) and (A-19),

$$N(z) = N_1 \frac{1 + k_2 C_+ (z - z_o)^n}{1 + C_+ (z - z_o)^n} \quad \text{for } z \geq z_o$$

$$N(z) = N_1 \frac{1 + k_2 C_- (z_o - z)^n}{1 + C_- (z_o - z)^n} \quad \text{for } z \leq z_o \tag{A-28}$$

where

$$n = k_1 - k_2 \tag{A-29}$$

If $N_1 \gg N_o$, $\eta \gg 1$. Then $k_1 = 1$, $k_2 = 0$, and $n = 1$. Equation (A-28) reduces to

$$N(z) = \frac{N_1}{1 + C_{\pm} |z - z_o|} \tag{A-30}$$

where C_+ is associated with positive values of $(z - z_o)$ and C_- with negative values, as in (A-28).

The integration constants C_+, C_- are determined by the boundary conditions. Let z_+ denote the height of the first node of the function $w(z)$ above the one at z_o. Since there is no flux of ionization across the planes $z = z_o$, $z = z_+$,

$$\int_{z_o}^{z_+} \alpha N^2 dz = \int_{z_o}^{z_+} q dz = \alpha N_o^2 (z_+ - z_o) \tag{A-31}$$

If $\eta \gg 1$, the integral of N^2 depends almost entirely on the form of $N(z)$ in the neighborhood of $z = z_o$, where it is given by Equation (A-30). From (A-30) and (A-31) we obtain

$$C_+ = \eta^2 (z_+ - z_o)^{-1} \tag{A-32}$$

whence

$$N(z) = \frac{\eta N_o}{1 + \eta^2 [(z-z_o)/(z_\pm - z_o)]} \tag{A-33}$$

Hence z_- denotes the level of the first node of the function $w(z)$ below the one at z_o.

Equation (A-33) shows that, except in the neighborhood of the peak, the electron density is smaller than the unperturbed density by a factor of order η. It also follows from (A-33) that the integrated electron density in the height range (z_o, z_+) is reduced from the unperturbed value by the factor

$$\frac{\int_{z_o}^{z_+} N dz}{\int_{z_o}^{z_+} N_o dz} = \frac{2 \ell n \, \eta}{\eta} \tag{A-34}$$

Bearing in mind that diffusion will considerably reduce the maximum value of $N(z)$ from the value ηN_o given by (A-33), we see that an electron-density peak forms chiefly through the erosion of the profile on either side of the peak.

$N(z)$ assumes the unperturbed value N_o when $z - z_o \approx \eta(z_+ - z_o)$. At this level the electron-density gradient is given by

$$\left(\frac{dN}{dz}\right)_{\pm} = - \frac{N_1}{z_{\pm} - z_o} \qquad (N = N_o) \tag{A-35}$$

A.4 EFFECTS OF DIFFUSION

Neglect of diffusion is valid as long as the magnitude of the second derivative d^2N/dz^2 is not too great. However, in the approximation that neglects diffusion entirely the electron-density gradient dN/dz is actually discontinuous at a peak. Diffusion therefore strongly influences the form of the electron-density profile in the immediate vicinity of a peak.

We are particularly interested in profiles for which $N_{max} \gg N_o$. Under this condition the ionization and recombination terms in Equation (A-15) are both negligible in comparison with the other terms in the equation, which accordingly reduces to

$$D \frac{d^2N}{dz^2} - w_o' z \frac{dN}{dz} - w_o' N = 0 \tag{A-36}$$

The appropriate solution of this equation is

$$N(z) = N_{max} \exp \left[\tfrac{1}{2} \frac{w_o'}{D} (z - z_o)^2\right] \tag{A-37}$$

N_{max} is determined by the condition

$$\int_{z_-}^{z_+} N^2(z)dz = N_o^2(z_+ - z_-) \equiv N_o^2 \lambda \tag{A-38}$$

Since the major contribution to the integral of N^2 over the range (z_-, z_+) comes from a narrow interval centered on z_o, we may use formula (A-37) to evaluate the integral in (A-38) to obtain

$$N_{max} = N_o \left[- \frac{w_o' \lambda^2}{\pi D} \right]^{\frac{1}{4}} \qquad \text{(A-39)}$$

Essentially the same formula has been derived by Whitehead[A-5] by a different argument. There is an important qualitative difference between the formula (A-39) for N_{max} with diffusion taken into account and the formula

$$N_{max} = N_1 = - \frac{w_o'}{\alpha} \qquad \text{(A-40)}$$

which holds when diffusion is neglected. When diffusion is taken into account, the ratio N_{max}/N_o is independent of N_o; when it is neglected, N_{max} itself is independent of N_o.

A.5 COMPARISON BETWEEN THEORY AND EXPERIMENT

A.5.1 The Value of N_{max}. In order to estimate N_{max}, we need to have an estimate of the drift gradient w_o'. If w is given by Whitehead's formula (A-12), w_o' is proportional to the vertical gradient of V_y the westward component of the neutral wind, the factor of proportionality being $(\omega_i/\nu_i) \cos\chi \approx 1/20$. On the assumption that the Hall current is fully inhibited, w is given by Equation (A-11), so that w_o' is proportional to the vertical gradient of the northward component of the neutral wind, the factor of proportionality being of order 1/2. Inspection of

the electron-density and wind profiles obtained in nearly simultaneous rocket experiments at nearly the same locations[A-3,A-9] shows that layers of enhanced ionization are associated with quite unremarkable wind shears -- of the order of 2×10^{-2} sec^{-1}. Consequently, we may take $-w_o'$ to be in the range

$$10^{-3} \leq - w_o' \leq 10^{-2} \qquad \text{(A-41)}$$

The value of the recombination coefficient α is rather uncertain. A. P. Mitra[A-10] gives the value

$$\alpha = 5 \times 10^{-8} \quad \text{(day)} \qquad \text{(A-42)}$$

Finally, N_o has the value

$$N_o = 1.5 \times 10^{5} \quad \text{(day)} \qquad \text{(A-43)}$$

These values are all in c.g.s. units, and all pertain to the level z = 100 km. From Equation (A-19) we see that the parameter η lies in the range

$$\frac{1}{10} \leq \eta \leq 1 \qquad \text{(A-44)}$$

where the upper and lower limits are associated with Equations (A-12) and (A-11) respectively. The corresponding range of the ratio N_1/N_o is, by Equation (A-17)

$$1 \leq \frac{N_1}{N_o} \leq 1.6 \qquad \text{(A-45)}$$

Since $N_1 \gg N_{max}$ in general, the low value of the ratio N_1/N_o indicated by (A-45) suggests that, during the day, vertical ionization drift does not give rise to significant perturbations of the electron-density profile.

As the nighttime values of both α and N_o are much smaller than the daytime values η (night) $\gg 1$, so that formula (A-39) applies. With the values

$$D = 2.5 \times 10^5 \tag{A-46}$$

$$10^6 \leq \lambda \leq 2 \times 10^6 \tag{A-47}$$

this yields

$$6 \leq \frac{N_{max}}{N_o} \leq 15 \tag{A-48}$$

which is in reasonable agreement with experiment. One cannot assert, however, that the drift mechanism will actually produce such high values of N_{max}/N_o, since the effects of wind variability have so far been neglected. Inspection of the wind data of Manring, Bedinger, and Knaflich[A-3] shows that in a 5 km height range centered on 100 km the direction of the wind vector frequently changes by $\pi/2$ or more. The same data show that at a given height the direction of the wind vector changes by 2π in about eight hours. Hence at this height any given feature of the wind profile has a vertical speed of about 2/3 m/sec. It follows that in general less than about 1.5×10^3 sec are available for the formation of a layer 1 km thick. The mean electron density of such a layer will exceed the unperturbed electron density by a factor not greater than $1.5 \times 10^3 \ |w_o'|$, so that, by (A-41)

$$\frac{\bar{N}}{N_o} \leq 1.5 \text{ if (A-12) applies;} \qquad \frac{\bar{N}}{N_o} \leq 15 \text{ if (A-11) applies} \tag{A-49}$$

where $\bar{N}$ denotes the mean electron density in a layer. As both limits in Equation (A-49) are upper bounds, this argument makes it seem unlikely that vertical ionization drift can produce the required degree of enhancement.

To sum up, the characteristic time associated with the building up of a peak in the electron-density profile by vertical ionization drift is either of the same order of magnitude as, or not much smaller than, the characteristic time associated with daytime recombination and with variations of the wind profile. It is therefore doubtful whether the drift mechanism can give rise to perturbations of the electron-density profile of the same magnitude as those associated with the phenomenon of sporadic E.

A.5.2 Shape of the Electron-Density Profile. Using a CW propagation technique, Seddon[A-2,A-11,A-12] has measured electron-density profiles for several E_s layers. L. G. Smith[A-1,A-9] has fully confirmed Seddon's findings, using an entirely different experimental technique (DC probe). The following properties of E_s layers appear to be well established. (1) The thickness of a typical E_s layer is between 500 and 2000 meters. Thick layers often resolve into two or more distinct thin layers. (2) The profile of a typical E_s layer has very steep sides. Typical gradients are of the order 10^5 to 10^6 (el cm^{-3} km^{-1}). (3) E_s layers are superimposed on an apparently unperturbed background. There is no evidence for any substantial reduction of electron density on either side of a layer. (4) Although layers of enhanced ionization

are nearly uniform in thickness, the ratio N_{max}/N_o varies over a wide range (1-100). Let us compare these experimental results with the corresponding predictions of the wind-shear theory.

(1) According to Equation (A-33), $\Delta z/\lambda \approx \eta$, where Δz is the thickness of a layer and λ is the vertical wavelength of the wind profile. Since $\lambda \approx 20$ km and $\Delta z \approx 1$ km, $\eta \approx 20$. This is very much higher than the daytime value predicted by theory.

(2) The predicted profile of an E_s layer has smoothly curving hyperbolic sides. According to Equation (A-35) the electron-density gradient is of order $2\eta N_o/\lambda = 2N_o/\Delta z$, which is smaller by a factor of 10 than commonly observed gradients.

(3) The wind-shear theory predicts that a substantial reduction in the "background" electron density must accompany the formation of a layer of enhanced density and that the integrated density in a height range of thickness λ is also substantially reduced. No such reduction seems to occur.

(4) The theory predicts a close relationship between the thickness of a layer and the ratio N_{max}/N_o. In the absence of diffusion $\Delta z \propto (N_{max}/N)^{-1}$; diffusion tends to reduce the range of variation of N_{max}/N_o. Hence the thickness Δz should vary over a wide range; in fact, it varies hardly at all.

A.5.3 Detailed Comparison Between the Wind Profile and the Ionization Profile. On three occasions in 1962 (7 November, 30 November,

and 5 December) teams headed by L. G. Smith and by E. Manring[A-9] obtained nearly simultaneous records of the ionization and wind profiles in the height range 80-130 km over Wallops Island, Virginia. The ionization profiles showed several thin, sharply defined layers of enhanced ionization, some of which could be identified with sporadic E layers recorded on ionograms.* It will suffice to consider the records of 7 November, which are extraordinarily rich in information.

The two ionization records of 7 November (one obtained during the ascent of the rocket, the other during the descent) show seven well-defined layers of enhanced ionization between 90 and 125 km. The intervals between successive peaks are virtually identical on the two records, but the zero-points of the two height scales differ by 3/4 km. Since the height measurements are based on radar observations of the rocket, they are more accurate for the ascent than for the descent. I have accordingly adopted the height scale determined for the ascent in the following discussion.

The height scale of the wind measurements is probably accurate to less than 1 km. The height discrimination of the wind measurements is about 1/2 km. Height discrimination of this order is actually needed to resolve the fine structure of wind profiles between 85 and 135 km.

*The horizontal separation between the ionospheric regions probed by the rockets on the one hand and the ionosonde on the other was of the order of 70-80 km.

Figures A-1 and A-2 show the ionization and wind profiles for 7 November 1962. The horizontal lines in Figure A-2 indicate the heights of the seven electron-density peaks that occur on both ionization records. The fine structure that appears in Figure A-2, i.e., the structure whose vertical scale is $\leq$ 2 km, is undoubtedly real and is a normal feature of wind profiles in this height range. Figure A-2 shows that there is a striking correspondence between the fine structure of the wind profiles and the fine structure of the electron-density profile: layers of enhanced ionization coincide with narrow regions where both the speed and direction of the wind are stationary, i.e., regions of zero shear. These narrow, zero-shear regions appear as transition layers between regions in which the shear is more or less constant.*

According to the wind-shear theory, the occurrence of layers of enhanced ionization should be related to the coarse structure of the wind profiles rather than to the fine structure, since the ionization that appears in these layers is supposed to be drawn from a region several times as thick as the layer. Let $\overline{\underset{\sim}{V}}(z)$ denote the mean value of $\underset{\sim}{V}$ in (say) a three-kilometer region centered on z. $\overline{\underset{\sim}{V}}(z)$ is a smoothly varying function of height with a vertical "wavelength" of about 15 km. If the wind-shear theory were correct, it would be possible to find a constant vector $\underset{\sim}{a}$ such that $\underset{\sim}{a} \cdot \overline{\underset{\sim}{V}} = 0$, and $\underset{\sim}{a} \cdot (d\overline{\underset{\sim}{V}}/dz) \ll 0$ at every electron-density peak.

*A theory that accounts for the correspondence between the fine structure of the ionization profile and the fine structure of the wind profiles will be described in another paper.

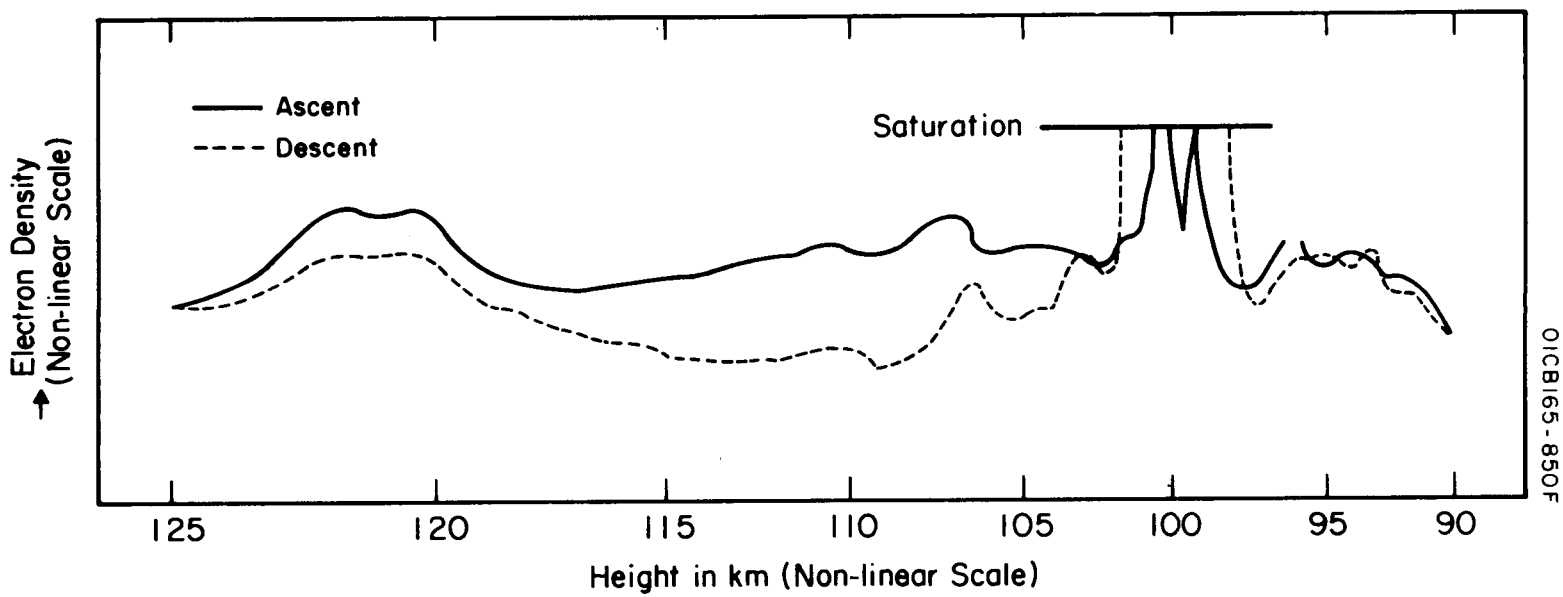

Figure A-1. Langmuir probe measurements by L. G. Smith of electron density over Wallops Island, Virginia, 0525 EST, 7 November 1962.

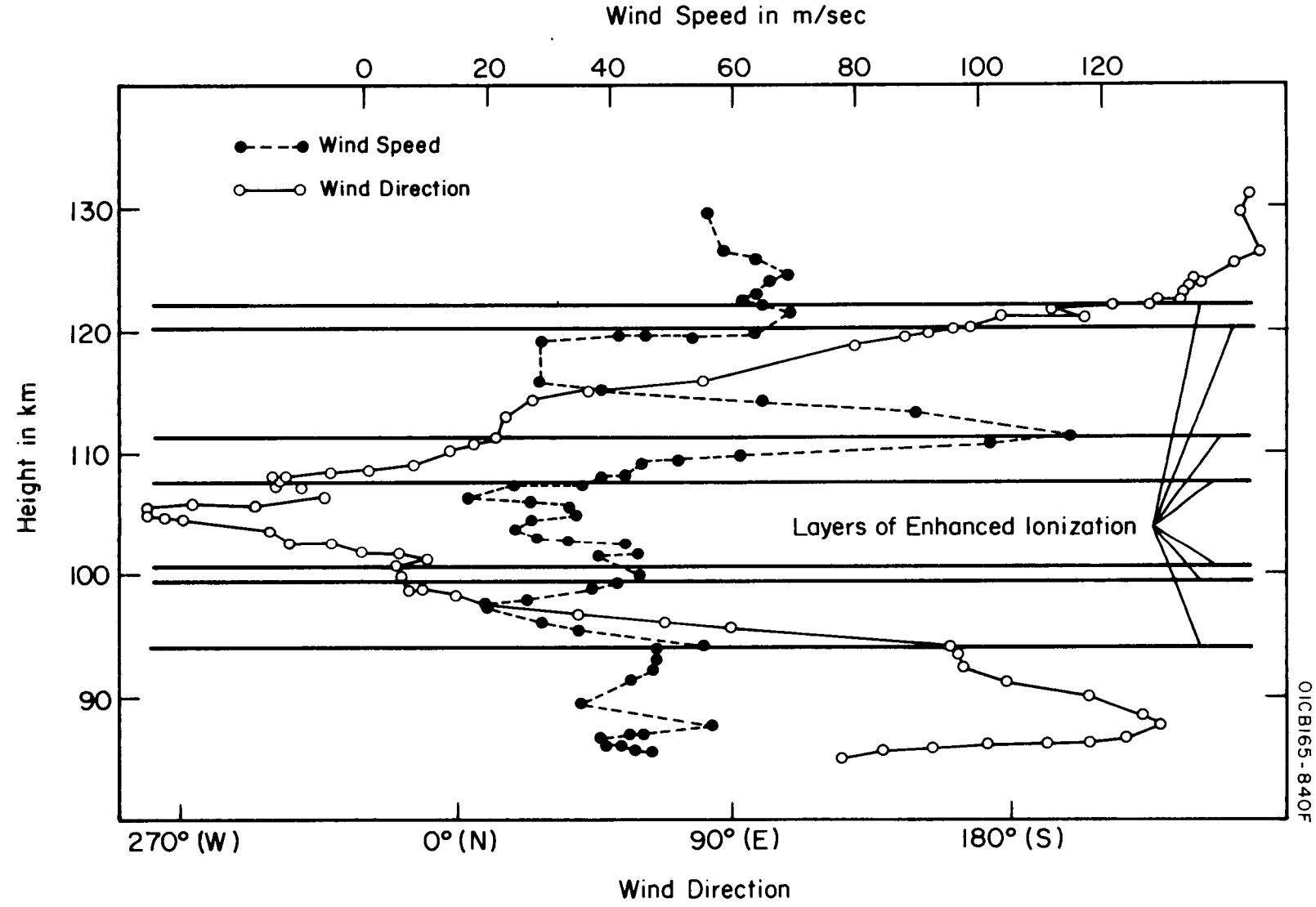

Figure A-2. Horizontal winds over Wallops Island, Virginia, from measurements by E. Manring, J. F. Bedinger, and H. Knaflich of a rocket-laid sodium trail, 0553 EST, 7 November 1962.

These requirements cannot be fulfilled with the data shown in Figure A-1, which require that $a_x \approx 0$, $a_Y < 0$ at 100 and 120 km, $a_x \approx 0$, $a_Y > 0$ at 111 km, and $|a_x| > |a_Y|$ at 107 km. Thus the wind-shear theory cannot account for all the layers of enhanced ionization that appear on the records of 7 November.

The records for 30 November and 5 December support the conclusions drawn from the record of 7 November: there is a close correspondence between the fine structure of the ionization profile and the fine structure of the wind profiles, layers of enhanced ionization tending to coincide with narrow layers of zero shear separating constant-shear regions; but there is no obvious connection between the gross structure of the wind profiles and the fine structure of the ionization profile.

A.5.4 Conclusions. The preceding discussion shows that the effects produced by vertical ionization drift are quantitatively too small and qualitatively not of the right kind to account for the narrow, well-defined layers of enhanced ionization associated with the phenomenon of sporadic E. Nevertheless, vertical ionization drift may be responsible for some less conspicuous features of ionization profiles in the E-region, especially at night. It will be easier to assess the role of vertical ionization drift once the primary mechanism for producing enhanced ionization in narrow layers is understood.

A.6 CRITIQUE OF THE TRAPPING HYPOTHESIS

Rawer[A-13] and Layzer[A-14] have independently suggested that some kind of meteorological discontinuity might act as a trap for vertically drifting ionization. Layzer gave theoretical reasons for believing that if true hydrodynamic turbulence exists in the E region it is confined to thin layers where the wind shear takes on exceptionally high values. Such thin turbulent layers might act as ionization traps, since turbulent mixing would tend to inhibit ionization drift across the layer. However, the experimental results described in the preceding section show that this hypothesis cannot be correct. Layers of enhanced ionization occur, in fact, in regions where the wind shear is exceptionally low. Indeed, the wind data give no indication of the existence of any kind of meteorological discontinuity whatever.

The trapping hypothesis is also difficult to reconcile with the extremely high ionization gradients characteristic of E_s layers and with the occurrence of multiple layers.

A.7 CONCLUSION

The preceding discussion supports the suggestion that vertical ionization drift produces observable changes of some kind in the ionization profile in the E region, particularly at night. But these changes are almost certainly not the sharply defined spikes associated with the phenomenon of sporadic E.

REFERENCES

A-1. Smith, L. G., "Rocket Measurements in the Nighttime Ionosphere," GCA Technical Report No. 62-1-N (1962).

A-2. Seddon, J. C., "Sporadic E as Observed with Rockets," in Ionospheric Sporadic E, Edited by E. K. Smith, Vol. 2, pp. 78-88, Pergamon Press, Oxford (1962).

A-3. National Aeronautics and Space Administration, Contract NASw-396, Final Report, "Study of Winds, Diffusion, and Expansion of Gases in the Upper Atmosphere," GCA Technical Report No. 63-16-N (May 1963).

A-4. Whitehead, J. D., "The Formation of a Sporadic-E Layer from a Vertical Gradient in Horizontal Wind," in Ionospheric Sporadic E, Edited by E. K. Smith, Vol. 2, pp. 276-291, Pergamon Press, Oxford (1962).

A-5. Whitehead, J. D., "The Formation of the Sporadic-E Layer in the Temperate Zones," J. Atmospheric Terrest. Phys., 20, 49-58 (1961).

A-6. Axford, W. I., "The Formation and Vertical Movement of Dense Ionized Layers in the Ionosphere Due to Neutral Wind Shears," J. Geophys. Res. 68, 769-779 (1963).

A-7. Martyn, D. W., "Electric Currents in the Ionosphere, 3, Ionization Drift Due to Winds and Electric Fields," Phil. Trans. Roy. Soc. London, A, 246, 306-320 (1953).

A-8. Baker, W. G., "Electric Currents in the Ionosphere, 2, The Atmospheric Dynamo," Phil. Trans. Roy. Soc., London, A, 246, 295-305 (1953).

A-9. Smith, L. G., "Measurements of Electron Density Profile in the Nighttime E Region," Geophys. Corp. of Am. Rept. NASw-489 (1963).

A-10. Mitra, A. T., "Night-time Ionization in the Lower Ionosphere, 1, Recombination Processes," J. Atmospheric Terrest. Phys. 10, 140-152 (1957).

A-11. Seddon, J. C., "Propagation Measurements in the Ionosphere with the Aid of Rockets," J. Geophys. Res., 58, 323-335 (1953).

A-12. Seddon, J. C., "Electron Densities in the Ionosphere," J. Geophys. Res., 59, 463-466 (1954).

A-13. Rawer, K., "Structure of E_s at Temperate Latitudes," in Ionospheric Sporadic E, Edited by E. K. Smith, Vol. 2, pp. 291-343, Pergamon Press, Oxford (1962).

A-14. Layzer, D., "The Turbulence Criterion in Stably Stratified Shear Flow and the Origin of Sporadic E," in Ionospheric Sporadic E, Edited by E. K. Smith, Vol. 2, pp. 258-275, Pergamon Press, Oxford (1962).